ACS OMEGA

Open Access

http://pubs.acs.org/journal/acsodf

Article

(Re-)Viewing Role of Intracellular Glucose Beyond Extracellular Regulation of Glucose-Stimulated Insulin Secretion by Pancreatic Cells

Firdos,[§] Tapabrata Pramanik,[§] Prachi Verma, and Aditya Mittal*

Cite This: *ACS Omega* 2024, 9, 11755−11768

Read Online

ACCESS | Metrics & More | Article Recommendations | Supporting Information

ABSTRACT: For glucose-stimulated insulin secretion (GSIS) by pancreatic β-cells in animals, it is believed that ATP generated from glucose metabolism is primarily responsible. However, this ignores two well-established aspects in literature: (a) intracellular ATP generation from other sources resulting in an overall pool of ATP, regardless of the original source, and (b) that intracellular glucose transport is 10- to 100-fold higher than intracellular glucose phosphorylation in β-cells. The latter especially provides an earlier unaddressed, but highly appealing, observation pertaining to (at least transient) the presence of intracellular glucose molecules. Could these intracellular glucose molecules be responsible for the specificity of GSIS to glucose (instead of the widely believed ATP production from its metabolism)? In this work, we provide a comprehensive compilation of literature on glucose and GSIS using various cellular systems - all studies focus only on the extracellular role of glucose in GSIS. Further, we carried out a comprehensive analysis of differential gene expression in Mouse Insulinoma 6 (MIN6) cells, exposed to low and high extracellular glucose concentrations (EGC), from the existing whole transcriptome data. The expression of other genes involved in glycolysis, Krebs cycle, and electron transport chain was found to be unaffected by EGC, except *Gapdh*, *Atp6v0a4*, and *Cox20*. Remarkably, 3 upregulated genes (*Atp6v0a4*, *Cacnb4*, *Kif11*) in high EGC were identified to have an association with cellular secretion. Using glucose as a possible ligand for the 3 proteins, computational investigations were carried out (that will require future 'wet validation', both in vitro and in vivo, e.g., using primary islets and animal models). The glucose-affinity/binding scores (in kcal/mol) obtained were also compared with glucose binding scores for positive controls (GCK and GLUT2), along with negative controls (RPA1, KU70−80, POLA1, ACAA1A, POLR1A). The binding affinity scores of glucose molecules for the 3 proteins were found to be closer to positive controls. Therefore, we report the glucose binding ability of 3 secretion-related proteins and a possible direct role of intracellular glucose molecules in GSIS.

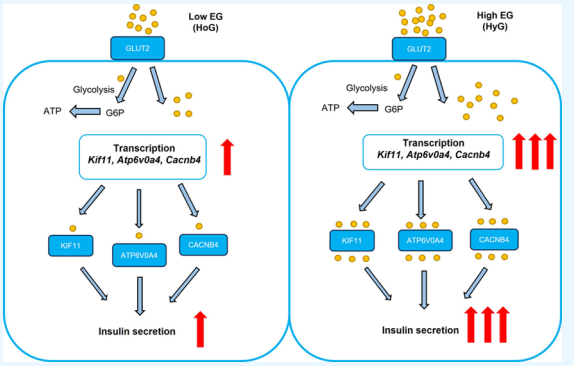

INTRODUCTION

Diabetes mellitus is a metabolic disease resulting from impaired glucose sensing, dampened insulin activity, or an absolute pancreatic β-cell destruction. As per the reports of the International Diabetes Federation (IDF), there were 537 million diabetics worldwide in 2021, which is expected to reach 643 million by 2030 and 783 million by 2045.[1] Diabetes mellitus (DM) can be classified as Type 1 and Type 2, respectively. Although accounting for only 5−10% of the total diabetic individuals, Type 1 DM is often fatal, characterized by an autoimmune pancreatic β-cell destruction, which leads to absolute insulin deficiency.[2] Type 2 DM is a chronic metabolic disease that happens due to genetic as well as acquired factors, resulting in impaired pancreatic β-cell functions as well as tissue insulin insensitivity.[3,4] A decrease in both pancreatic β-cell mass and insulin secretory granules has been reported.[5] In fact, a 60% decrease in pancreatic β-cell mass with an associated decrease in GSIS is also known.[6,7] Impaired insulin secretion leads to hyperglycemia with an adverse effect on internal organs and complications like retinopathy, nephropathy, neuropathy, cardiovascular disease, and sexual abnormalities.[8,9] Inter- and intraislet cellular communication-regulated insulin secretion is required to maintain a basal level of insulin and stimulate GSIS response.[10] Glucose metabolism through glycolysis is performed by glucokinase (GCK), which is an isoform of hexokinase, termed hexokinase IV-β. This enzyme has been known to be the "glucose sensor" in pancreatic β-cells, performing the rate-limiting step of glucose phosphorylation.[11] Glucose can regulate glucokinase activity, thereby

Received: November 17, 2023
Revised: January 31, 2024
Accepted: February 7, 2024
Published: February 29, 2024

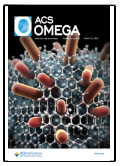

Table 1. Different Insulin-Secreting Model Systems Obtained from Different Species Used to Study GSIS

source or species	type of cells	cells	doubling time	GSIS response	role of glucose behind GSIS (extracellular or intracellular)	refs
hamster	cell lines	HIT	34 h	For HIT cells, a low GSIS response is observed as compared to primary islets. The doubling time of INS-1, INS1 832/13, and INS-1E cells ranges from 82 to 166 h; thus, subculturing would be time-consuming, although they show GSIS at physiological glucose level. Insulin secreted per 10^6 cells per h for BRIN-BD11, RINr, RINm, and RINm5F cells is considerably low. CRI-G1 is not responsive toward physiological glucose level. MIN6 shows comparable GSIS to that of islets and insulin secreted per 10^6 cells per hr is considerably high. βTC-1, NIT-1, and IgSV195 cells are not responsive toward physiological glucose level. The doubling time of EndoC-βH1 cells is 120 h; thus, subculturing would be time-consuming. βlox5 cells show a low insulin content. CM and TRM-1 do not show GSIS.	extracellular	44
rat		INS-1, INS1 832/13, INS-1E, BRIN-BD11, RINr, RINm, RINm5F, CRI-G1	82−166 h			45−51
mouse		MIN6, βTC-1, βTC-6, NIT-1, IgSV195, βHC9	48−58 h,			26,52−56
human		EndoC-βH1, βlox5, CM, TRM-1, NAKT-15	120 h			57−62
hamster	islets	primary islets	NA	Subculturing of primary islets is often limited by availability of endocrine tissue. The GSIS response seen in some cell lines was comparable to that of the islets. The observed fold change in GSIS varied between the islet species when treated with different EGC's.	extracellular	44
rat						63
mouse						63,64
human						64

https://doi.org/10.1021/acsomega.3c09171
ACS Omega 2024, 9, 11755−11768

regulating glucose usage as well as GSIS in pancreatic β-cells.[12] Hence, GCK proteins are also well-established glucose interactors. The transport of glucose into the β-cells is not rate limiting, executed by the glucose transporters GLUT1 or GLUT2, depending on the species, human or rodent, respectively. This rapid transport of glucose results in an equilibrium between the extracellular and the intracellular glucose molecules. Hence, GLUT proteins are also well-established glucose interactors.[13−15] As is known, insulin secreted from the β-cells of the pancreatic islets utilizes extracellular glucose, which is required for metabolic energy. Also, prevalent views on insulin secretion by pancreatic β-cells in animals are known to be dependent on the extracellular glucose concentration stimulus as the triggering signal behind GSIS. This is due to glucose metabolism that generates ATP, followed by closure of K_{ATP} channels and opening of Ca^{2+} channels that elevate cytosolic Ca^{2+}, accounting for exocytosis of insulin granules and, subsequently, the first phase of insulin secretion.[16−18] However, ATP generation or a rise in the ATP/ADP ratio may happen from other intracellular pathways also. Thus, the specificity of glucose in GSIS is not attributable to ATP from glucose metabolism alone; in fact, the reason behind this specificity remains undiscovered to date. The amplifying signal of GSIS that accounts for the second phase of insulin secretion is tightly regulated by glucose and dependent on the metabolism of glucose, and glucose can independently enhance insulin secretion due to its effect on K_{ATP} channels.[19−21] Both the phases of GSIS happen due to the movement of "restless newcomers" or the "readily releasable pool" of insulin granules as well as the "reserve pool" of insulin granules that engage upon glucose stimulus and fuse to the plasma membrane of pancreatic β-cells.[22] It has also been reported that the rate of intracellular glucose transport by GLUT proteins surpasses glucose phosphorylation rate by 100 times.[23] There is limited knowledge about these transported but unphosphorylated glucose molecules. As a matter of fact, no direct link has been established until date between glucose and insulin secretion. In straightforward words, why is GSIS considered to be glucose specific only, i.e., what are the direct roles of glucose molecules in triggering as well as amplifying GSIS? To investigate these questions, we hypothesized that intracellular (unphosphorylated) glucose molecules are somehow involved in the regulation of insulin secretion. While there have been regular attempts to gain insights into the regulatory action of glucose and insulin secretion specifically pertaining to 'extra-pancreatic-cell-homeostasis' and signaling pertaining to the role of glucose amplification behind GSIS and as a "surface ligand" behind triggering of GSIS, the intracellular role of glucose has been attributed to generation of ATP primarily due to its metabolism.[24,25] We move beyond the "convention". Our work specifically addresses the possible role of intracellular glucose in the β-cells.

To test the hypothesis as explained above, and as mentioned in Table 1, we used an experimental system whose GSIS was comparable to that of mouse islets (275 mU/10^6 cells/24 h at 25 mM glucose stimulus) and has provided significant insights into GSIS over the years, i.e., the cell culture model system of Mouse Insulinoma 6 (MIN6) cells.[26,27] From whole transcriptome studies of Min6 cells exposed to extracellular hyperglycemic conditions, we identified the upregulation of 3 secretion-specific genes corresponding to the proteins KIF11, ATP6V0A4, and CACNB4. KIF11, also known as Kinesin-related motor protein Eg5, mediates secretory protein transport to the cell membrane from the Golgi complex through the transport of Rab6 containing CARTS,[28] expanded as carriers of trans-Golgi to the cell surface toward the cell membrane through the course of protein secretion.[29] CACNB4, one of the $Ca_V\beta4$ auxiliary subunits, remains attached to the transmembrane $Ca_V\alpha1$ subunit, thereby making up the functional Ca_V voltage-dependent calcium channel staged on the pancreatic β-cell membrane. These channels regulate β-cell insulin secretion.[30−33] Mutation at the a3 locus or loss of function of the a3 isoform of V-type ATPase dampened insulin secretion in the isolated islets of oc/oc mice, indicating that the protein participates in the exocytosis of insulin secretory vesicles.[34] Also, the a4 isoform of V-type ATPase has been found to be expressed in kidneys regulating acid−base equilibrium.[35] Based on our transcriptome data that showed upregulation of the a4 isoform of V-type ATPase, we assumed that this protein might be involved in insulin secretion along with the a3 isoform. The question that we aimed to address is whether these proteins sequester glucose or not. Using AutoDock Tools 4.2.6 (http://autodock.scripps.edu; ADT), glucose was investigated as a possible ligand for the above 3 proteins; the docked conformations were subsequently visualized using Discovery Studio 2021 (https://discover.3ds.com/discovery-studio-visualizer-download; DS). ADT is a docking program based on the Lamarckian genetic algorithm (LA). A free energy force field creates or predicts conformations of 10 docked ligand poses with their corresponding binding energies. The force field includes six pairwise evaluations (V), including respective sets of bound and unbound ligand (L), protein (P), and protein−ligand (P-L) conformations. The pairwise evaluations consider parameters consisting of repulsion, hydrogen bonding, electrostatics, and desolvation.[36−40] For proteins not resolved entirely by X-ray, NMR, or EM, AlphaFold-predicted protein structures were used from AlphaFold[41] protein structure Database v2.0 (https://alphafold.ebi.ac.uk/).

RESULTS AND DISCUSSION

Model Systems for Insulin Secretion that Mimic Pancreatic β-Cell Physiology. To emphasize the role of internalized and nonphosphorylated glucose molecules behind GSIS, we compiled a list of different insulin-secreting model systems that are known to perform GSIS and also looked into the role of glucose behind the same, as shown in Table 1. This includes cell lines and primary islets. In Table S14, we have shown Table 1 in detail. This includes the name (source or species) of the model systems and the procedure by which they were isolated, the stimulus method behind GSIS, extent of maximum insulin content or secretion, type of insulin assay, extent of fold change observed as a response to GSIS, and the role of glucose behind GSIS, with appropriate references. Each of the model systems has its own unique properties, which relate to pancreatic β-cell physiology or function. Starting with primary rat, hamster, mouse, human islets, or well-established cell lines, we also review nonislet cells engineered to produce insulin.[42,43]

Compared to MIN6 cells, some of the cell lines secreted lower insulin (in terms of mU/10^6 cells/h); some were unresponsive to glucose stimulation beyond a certain stimulus; and some did not exhibit GSIS at physiological glucose concentration, or did not show a considerable fold change in GSIS at increasing glucose concentrations. Since MIN6 cells have a doubling time of 48 h as opposed to 82−166 h of rat

https://doi.org/10.1021/acsomega.3c09171
ACS Omega 2024, 9, 11755−11768

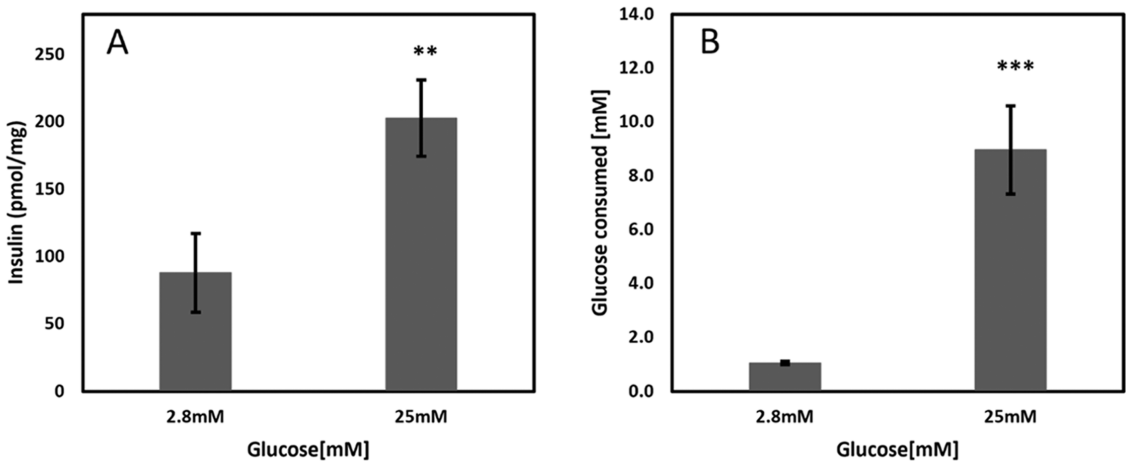

Figure 1. Insulin secretion and glucose consumption by MIN6 cells under HoG and HyG conditions. (A) Fold change in insulin secretion after treatment with 2.8 and 25 mM extracellular glucose. (B) Glucose consumption by cells, calculated by measuring the residual glucose concentration in the culture medium after 1 h of incubation with the initially supplied glucose concentrations of 2.8 and 25 mM extracellular glucose.

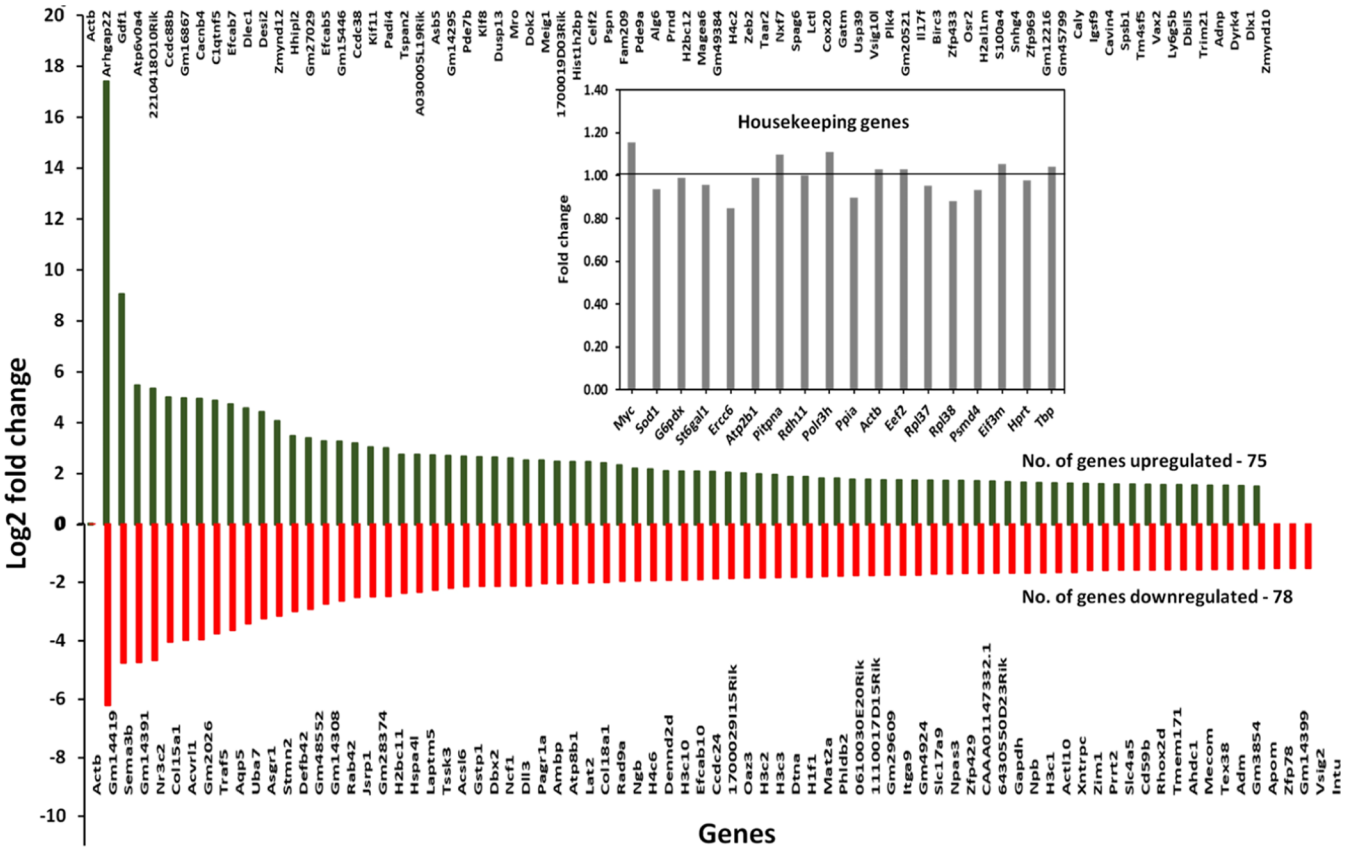

Figure 2. Transcriptome analyses of MIN6 cells under HoG and HyG conditions. The log 2 fold change (log 2 fc) was set at a threshold of ±1.5; 75 protein-coding genes were upregulated and 78 protein-coding genes were downregulated at high EGC, in terms of FPKM. The inset shows control transcriptome analyses - housekeeping genes are relatively unaffected in HoG and HyG conditions (only fold changes are shown to highlight the very minor variabilities observed).

insulinoma cells or 120 h of human insulinoma cells, they are convenient for subculturing. As mentioned earlier, MIN6 cells secrete a considerable amount of insulin (275 mU/10^6 cells/24 h at 25 mM EGC), which is comparable to that of mouse islets. Not only do they respond to physiological glucose levels but they also show enhanced GSIS with a significant fold change at incremental EGCs. Thus, all of these factors consolidate MIN6 cells as a robust in vitro model system for studying pancreatic β-cell physiology.

Insulin Secretion. MIN6 cells have been triggered by 2.8 and 25 mM extracellular glucose concentrations. Figure 1A shows increased insulin secretion when treated with 25 mM extracellular glucose, as opposed to 2.8 mM extracellular glucose. Glucose consumption was calculated by measuring the residual glucose concentration in the culture medium after 1 h

https://doi.org/10.1021/acsomega.3c09171
ACS Omega 2024, 9, 11755−11768

Table 2. Selection of Protein Structures: The Protein Structures Used for Glucose Binding Analyses through ADT

gene	protein	residues	organism	PDB/UniProt accession
KIF11	kinesin-like protein	1052	*Mus musculus*	Q6P9P6
KIF11	kinesin-like protein	1056	*Homo sapiens*	P52732
CACNB4	voltage-dependent L-type calcium channel subunit β-4	519	*M. musculus*	Q8R0S4
CACNB4	voltage-dependent L-type calcium channel subunit β-4	520	*H. sapiens*	O00305
ATP6V0A4	V-type proton ATPase116 kDa subunit a isoform 4	833	*M. musculus*	Q920R6
ATP6V0A4	V-type proton ATPase116 kDa subunit a isoform 4	840	*H. sapiens*	Q9HBG4
GCK	hexokinase 4	465	*M. musculus*	P52792
GCK	hexokinase 4	465	*H. sapiens*	1V4S/P35557
SLC2A2	solute carrier family 2, facilitated glucose transporter member 2	523	*M. musculus*	P14246
SLC2A2	solute carrier family 2, facilitated glucose transporter member 2	524	*H. sapiens*	P11168
RPA1	replication protein A 70 kDa DNA-binding subunit	623	*M. musculus*	Q8VEE4
RPA1	replication protein A 70 kDa DNA-binding subunit	616	*H. sapiens*	P27694
XRCC6/XRCC5	Ku70−80 heterodimer	A chain −609 B chain −565	*H. sapiens*	1JEQ
XRCC6	Ku70	608	*M. musculus*	P23475
XRCC6	Ku70	609	*H. sapiens*	P12956
XRCC5	Ku80	732	*M. musculus*	P27641
XRCC5	Ku80	732	*H. sapiens*	P13010
POLA1	DNA polymerase α catalytic subunit	1465	*M. musculus*	P33609
POLA1	DNA polymerase α catalytic subunit	1462	*H. sapiens*	P09884
ACAA1A	3-ketoacyl-CoA thiolase A, peroxisomal	424	*M. musculus*	Q921H8
ACAA1A	3-ketoacyl-CoA thiolase A, peroxisomal	424	*H. sapiens*	P09110
POLR1A	DNA-directed RNA polymerase I subunit RPA1	1717	*M. musculus*	O35134
POLR1A	DNA-directed RNA polymerase I subunit RPA1	1720	*H. sapiens*	O95602

of incubation with the initially supplied glucose concentration, as shown in Figure 1B. Insulin secretion increased up to 2.3-fold as compared to basal glucose level secretion. Next, we go through transcriptome studies to estimate the gene expression profile between HoG (2.8 mM) and HyG (25 mM) glucose concentrations, respectively.

Transcriptome Studies. In this work, we analyzed differential gene expression in MIN6 cells exposed to low and high extracellular glucose concentrations (EGC), from their whole transcriptome data (55,467 distinct transcripts, of which 14,427 were identified as successfully expressed genes).[65] The study of differentially expressed genes (DEGs) can be obtained with high precision when the true number of DEGs ranges from 15 to 30%, even in the absence of biological replicates.[66] We obtained a value of 26%; thus, our study of DEGs was precise enough. The data were submitted to the NCBI-GEO (National Center for Biotechnology Information − Gene Expression Omnibus) database repository with an assigned accession number record of GSE226652. The entire differential gene expression analyses study can be viewed through the link https://www.ncbi.nlm.nih.gov/geo/query/acc.cgi?acc=GSE226652 and reference[65]. As shown in Figure 2 (inset), the fold change of housekeeping genes is unaffected under both HoG and HyG conditions. We have taken these genes as controls to check for differentially expressed genes at different glucose treatments. The log 2 fold change (log 2 fc) was set at a threshold of ±1.5. In terms of FPKM, we found 75 protein-coding genes to be upregulated and 78 protein-coding genes to be downregulated, respectively, at high EGC, as shown in Figure 2 as well as Table S1a,b, respectively. Of these, we identified that only 3 out of the upregulated genes (*Atp6v0a4*, *Cacnb4*, *Kif11*) are involved in secretion. These 3 genes were upregulated in terms of both FPKM and TPM. So, we went forward with FPKM values based on our results. Remarkably, other than 3 (*Gapdh*, *Atp6v0a4*, and *Cox20*), the expression of genes associated with glycolysis, the TCA cycle, and ETC was found to be unaffected by EGC, as shown in Table S2. Thus, we report that glucose consumption as a nutrient is independent of EGC in GSIS.

Selection of Protein Structures, Glucose Binding Studies through ADT, and Subsequent Visualization of the Docked Conformations through DS. The protein structures used for glucose binding analyses were downloaded from RCSB PDB (https://www.rcsb.org/) and UniProt database (https://www.uniprot.org/). AlphaFold-predicted protein structures were used from AlphaFold protein structure Database v2.0 (https://alphafold.ebi.ac.uk/). The details are shown in Table 2. Truncated mouse KIF11 (residue 90−400) and truncated mouse CACNB4 (residue 60−450) were also used for glucose binding analyses.

The binding energies (kcal/mol) and the total number of interactions for the respective 10 conformations within a single protein as well as for every other protein molecule used are shown in Tables S6a,b, S7, and S8a,b, respectively. They have been categorized into 3 distinct protein sets: Test molecules identified by transcriptome analyses under hyperglycemic condition—KIF11 mouse, CACNB4 mouse, and ATP6V0A4 mouse as shown in Table S6a, and for truncated KIF11 (90−400) and truncated CACNB4 (60−450) as shown in Table S6b; positive controls, known interactors with glucose—GCK (human and mouse) and GLUT2 (human and mouse), as shown in Table S7; and negative controls, not known to interact with glucose—RPA1 human, KU70−80 human, POLA1 human, POLR1A human, and ACAA1A mouse, as shown in Table S8a,b, respectively. The highest binding energy values (kcal/mol) corresponding to a particular protein conformation have been shown in Table 3 for test molecules, positive controls, and negative controls. Accordingly, the two-dimensional (2D) diagram of the ligand-bound protein conformations that exhibited the highest binding energy values

https://doi.org/10.1021/acsomega.3c09171
ACS Omega 2024, 9, 11755−11768

Table 3. Summary of the Highest Glucose Binding Scores (kcal/mol) Obtained for the Respective Conformations of the Test Molecules, Positive Controls, and Negative Controls, Respectively

protein	conformation with the highest binding energy	binding energy (kcal/mol)
KIF11 mouse	10	−4.62
truncated KIF11 mouse (90−400 residues)	9	−4.56
CACNB4 mouse	6	−4.19
truncated CACNB4 mouse (*60−450* residues)	3	−4.46
ATP6V0A4 mouse	1	−4.09
GCK mouse	4	−5.70
GCK human	1	−7.16
GLUT2 mouse	9	−5.35
GLUT2 human	3 and 4	−4.64
RPA1 human	4	−3.81
KU70−80 human	9	−3.75
POLA1 human	4	−3.58
POLR1A human	7	−2.66
ACAA1A mouse	1 and 3	−2.82

along with the different interactions as obtained through DS have been shown in Figure 3A−E, corresponding to KIF11, CACNB4, ATP6V0A4, truncated KIF11 and truncated CACNB4 respectively; Figure 3F−J corresponding to human GCK, mouse GCK, third docked conformation of human GLUT2, fourth docked conformation of human GLUT2, and mouse GLUT2, respectively, and in Figure 3K−O corresponding to RPA1, KU70−80, POLR1A, ACAA1A, and POLA1, respectively. The highest binding energy corresponding to the respective conformation of the protein molecule along with the orientation or the binding propensity of the docked ligand (D-glucose) was chosen and is shown in Table S10.

Calculation of Pearson Correlation Coefficient (r). Pearson correlation coefficient (r) was calculated between the number of interactions for the respective conformations within a single protein molecule and the corresponding binding energies (kcal/mol) obtained. This was done for every other protein molecule used, as shown in Table S9. A scatter plot was drawn, as shown in Figure 4, which showed the number of interactions for every conformation within a single protein on the *X*-axis and the corresponding binding energy scores (kcal/mol) obtained on the *Y*-axis. This was done for all of the 14 protein molecules. Since binding energy should decrease and tend toward negative with increasing number of interactions as a stable ligand-protein interaction is achieved, one would expect a negative correlation between the 2 parameters for all of the protein molecules.

Binding Studies with Other Ligands. As described in the methodology for glucose binding analyses, binding studies were further done with hexophosphate ligands involved in glycolysis like G6P, F6P, and F16BP; epimers of glucose such as mannose and galactose; aldohexoses such as altrose, allose, gulose, idose, and talose, and ketohexoses such as fructose,

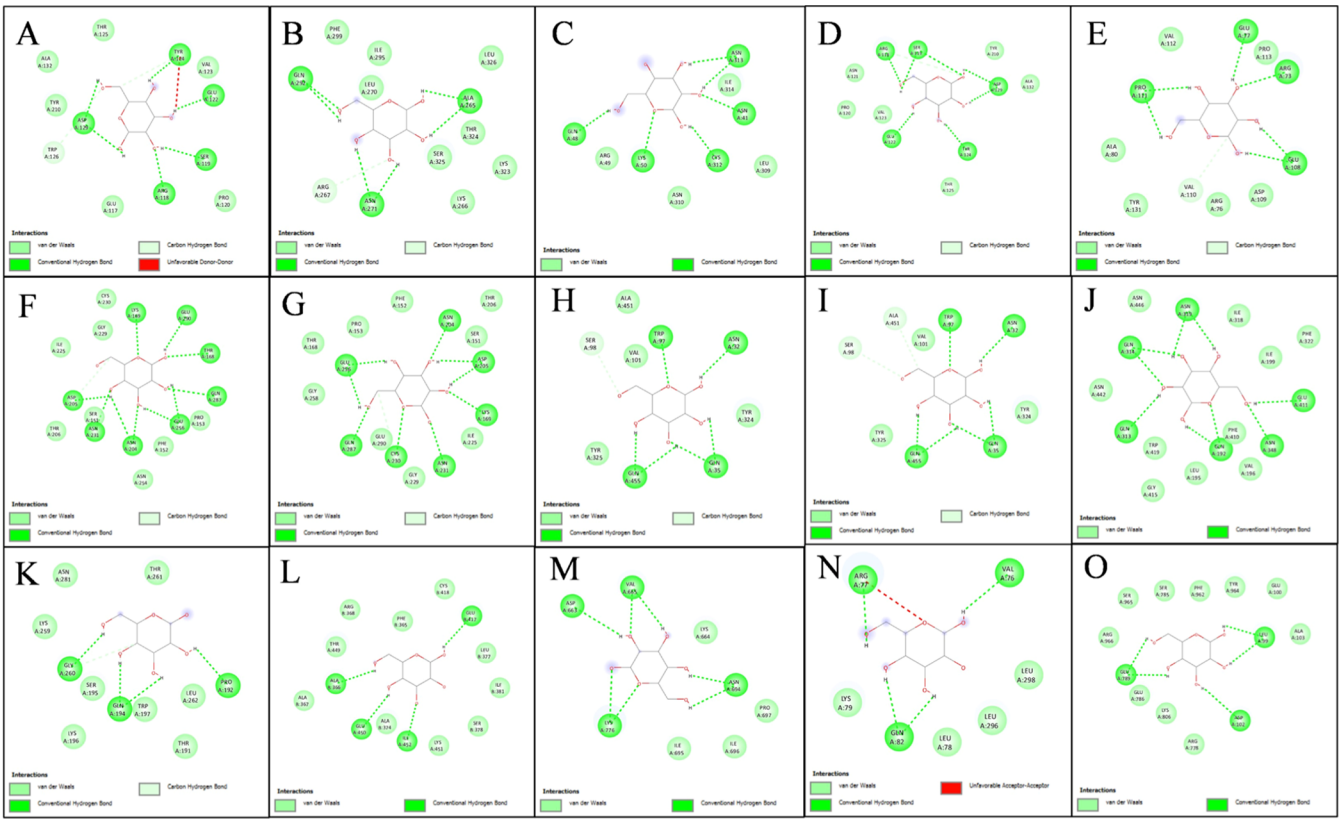

Figure 3. 2D diagrams of the ligand-bound protein conformations. The ligand is D-glucose and the proteins in (A−E) are KIF11, CACNB4, ATP6V0A4, tKIF11, and tCACNB4; these complexes were found to have the highest binding energy value scores (in kcal/mol). 2D diagrams of positive controls for the ligand-bound protein conformations; the proteins in (F−J) are human GCK, mouse GCK, 3rd conformation of human GLUT2, 4th conformation of human GLUT2, and mouse GLUT2, respectively. 2D diagrams of negative controls for the ligand-bound protein conformations; the proteins in (K−O) are RPA1, KU70−80, POLR1A, ACAA1A, and POLA1, respectively.

https://doi.org/10.1021/acsomega.3c09171
ACS Omega 2024, 9, 11755−11768

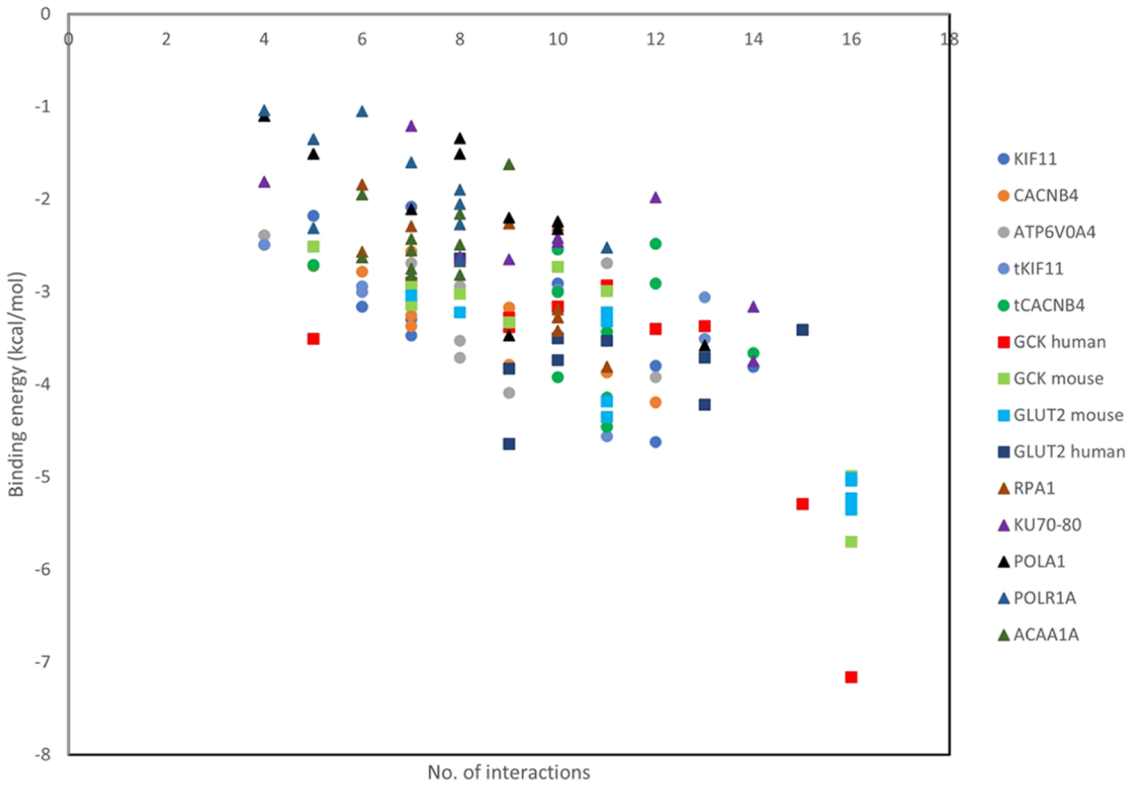

Figure 4. Decrease in value of binding energy with increasing number of interactions. The scatter plot shows the number of interactions for the respective 10 conformations of each protein molecule docked with glucose in the *X*-axis with their corresponding binding scores (kcal/mol) obtained in the *Y*-axis.

psicose, tagatose, and sorbose. The three-dimensional (3D) conformers of various ligands downloaded as .sdf files and used for binding studies have been shown in Table S11, with their respective PubChem CIDs (https://pubchem.ncbi.nlm.nih.gov/). The highest binding score obtained is indicated in parentheses alongside the corresponding conformation and is shown in Table S3. The binding scores obtained corresponding to the 10 docked conformations using the ligands as mentioned above have been shown in Table S3a−o, respectively, and the respective grid box parameters have been shown in Table S4a−o, respectively.

Comparison between the Binding Scores Obtained for Different Ligand-Protein Interactions. The highest binding score was shown by GCK (human −7.16 kcal/mol and mouse −5.7 kcal/mol, respectively) when docked with glucose, substantiating the fact that they are well-known glucose interactors. GLUT2 proteins (human −4.64 kcal/mol and mouse −5.35 kcal/mol, respectively) also showed a high binding score when docked with glucose, thus being well-known glucose interactors. Interestingly, the test proteins KIF11, CACNB4, and ATP6V0A4 showed binding scores of −4.62, −4.19, and −4.09 kcal/mol, respectively, when docked with glucose. These binding scores are closer to the glucose binding scores obtained for the positive controls. The negative controls RPA1, KU70−80, POLA1, ACAA1A, and POLR1A showed binding scores of −3.81, −3.75, −3.58, −2.62, and −2.66 kcal/mol, respectively, when docked with glucose. Surprisingly, mannose showed a binding score of −4 kcal/mol with GLUT2 mouse, and galactose showed a binding score of −4.05 kcal/mol with GLUT2 human, respectively. Psicose showed a binding score of −4.03 kcal/mol with GLUT2 human. Also, allose and talose showed a binding score of −4.13 and −4.09 kcal/mol, respectively, when docked with GCK human, and gulose showed a binding score of −4.18 kcal/mol with GCK mouse.

Relevance of Grid Box Size Dimensions with Key Glucose Binding Residues of Human Glucokinase and Glucose Binding Score (kcal/mol). For glucose binding analysis with human GCK, the grid box size or the axes dimension points were first set at $x = 40$, $y = 40$, and $z = 40$, respectively. The highest binding score thus obtained with glucose as the ligand was −4 kcal/mol, and subsequent analysis through DS, as shown in Figure 5D, showed Lys^{169} and Asp^{205} residues to be present in the glucose binding cavity. The grid box size was then increased to $x = 126$, $y = 126$, and $z = 126$, respectively. The highest binding score obtained with glucose as the ligand was −7.16 kcal/mol, and subsequent analysis through DS as shown in Figure 5A revealed Thr^{168}, Asn^{204}, Asn^{231}, Glu^{256}, and Glu^{290} to be present in the binding cavity residue along with Lys^{169} and Asp^{205}, participating in hydrogen bond formation with glucose. Interestingly, Glu^{256} is a key glucose binding residue in the active site of GCK. The natural GCK mutation at 256 E-K has been found in maturity-onset diabetes of the young (MODY2), and site-directed mutagenesis resulted in loss of glucose binding ability, rendering the enzyme catalytically inactive.[67−70]

Validating AutoDock's Computational Output. Human GCK complexed with glucose, PDB − 1V4S, was taken, as shown in Figure 5B. The 2D diagram of the number of interactions obtained with glucose as analyzed through DS is shown in Figure 5C. Now, glucose was docked with human GCK protein through ADT and the 2D diagram of the conformation exhibiting the highest binding score of −7.16 kcal/mol was analyzed through DS, as shown in Figure 5E,F.

https://doi.org/10.1021/acsomega.3c09171
ACS Omega 2024, 9, 11755−11768

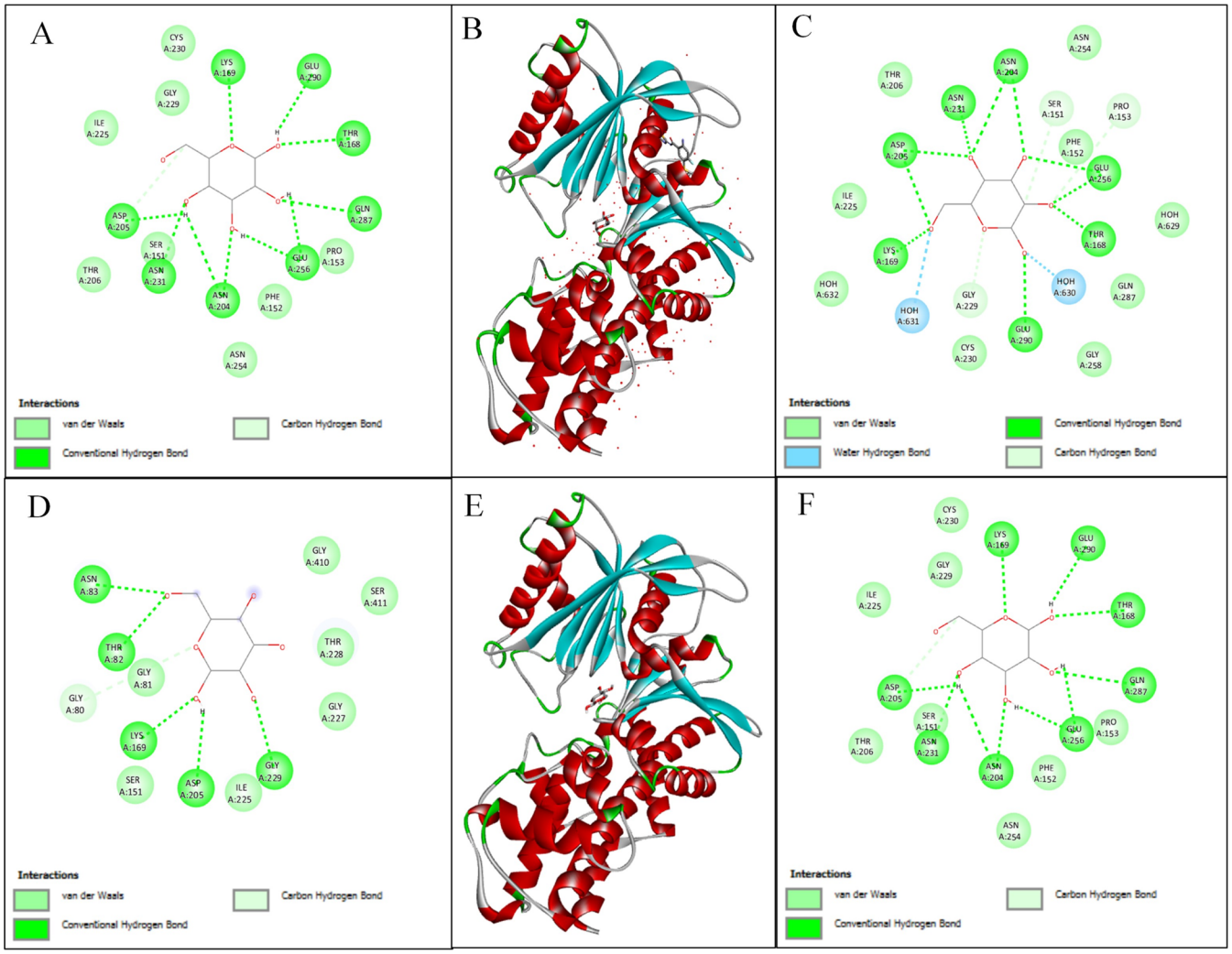

Figure 5. Relevance of the grid box size dimensions with the key glucose binding residues of human GCK protein and computation of glucose binding score (kcal/mol) along with validation of AutoDock's computational output. Human GCK protein interacting with glucose as analyzed through ADT and DS − Conformation 1 on the left (A) exhibiting the highest binding energy of −7.16 kcal/mol with all the 7 catalytic residues present, whereas only 2 catalytic residues are present (or 5 absent) in Conformation 4 at the bottom (D) exhibiting the highest binding energy of −4 kcal/mol. (B) shows the PDB structure (1V4S) of human GCK and (C) shows the interactions analyzed through DS. (E) shows conformation 1 of glucose-bound-human-GCK as obtained through ADT and (F) shows the interactions analyzed through DS.

The glucose binding pockets, as mentioned earlier, were remarkably similar in both Figure 5C and F involving the glucose-interacting residues Thr^{168}, Lys^{169}, Asn^{204}, Asp^{205}, Asn^{231}, Glu^{256}, and Glu^{290}.

Biological Validation of the Computational Results. To further validate AutoDock's computational output, experimentally obtained binding affinities between a particular protein and ligand in terms of K_m (mM) were categorized into positive and negative controls, and then were compared with the obtained binding scores in terms of kcal/mol of the same protein−ligand set. The protein−ligand sets are shown in Table 4, with appropriate references.[71−76] A linear regression scatter plot was drawn between the binding affinity values in terms of K_m (mM) in the *X*-axis and AutoDock's computational output (binding score values) in terms of kcal/mol in the *Y*-axis, as shown in Figure 6. A strong/greater binding affinity is characterized by a lower/lesser K_m, and this should correspond to a lower (more negative) binding score in terms of kcal/mol. This was seen from the scatter plot, which showed

Table 4. Biological Validation of Computational Results

control	protein−ligand	binding score obtained from AutoDock (kcal/mol)	binding affinity obtained from literature, K_m (mM)	refs
positive control	GCK-glucose, close	−7.16	6	73
	GCK-glucose, close	−5.7	6	73
	islet GLUT2-glucose	−5.35	17	74
	liver GLUT2-glucose	−4.64	19	72
negative control	GCK without glucose, super open	NA	30	76
	soybean β-amylase	NA	45	75
	GLUT2 fructose	−3.66	76	71
	GLUT2 galactose	−4.05	92	71
	GLUT2 mannose	−2.4	125	71

https://doi.org/10.1021/acsomega.3c09171
ACS Omega 2024, 9, 11755−11768

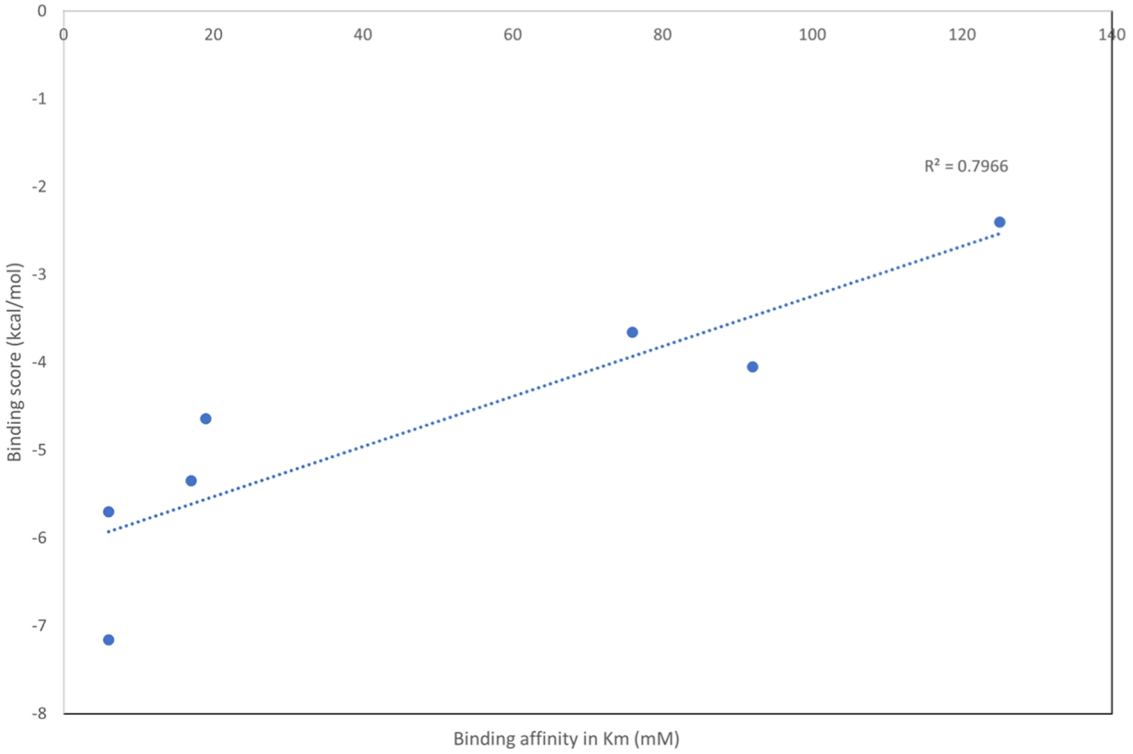

Figure 6. Biological validation of computational results. A linear regression scatter plot (R^2 = 0.79) between the experimental binding affinity values in terms of K_m in the *X*-axis and AutoDock-obtained binding scores in terms of kcal/mol in the *Y*-axis.

an R^2 value of 0.79 or 0.88 (data not shown), thus indicating a linear relationship between the two parameters.

Comparison between the Glucose Binding Scores Obtained with the Test Proteins and the Binding Scores Obtained with Other Ligands. The highest binding scores (kcal/mol) obtained with the test proteins using glucose as the ligand were statistically compared with the highest binding scores (kcal/mol) obtained with the test proteins for every other ligand, using two-tailed Student's *t* test assuming equal variances. The p-values thus obtained are shown in Table S12. Interestingly, none of the glycolytic metabolites or hexose sugars exhibited a similarity with respect to the glucose binding scores.

Comparison of Glucose Binding Scores between Homologous Proteins. Homologous proteins belonging to the same protein sets were chosen that were previously not used for binding studies, and then, binding studies were done specifically using glucose as the ligand for comparison. The glucose binding scores as obtained are shown in Table S13a. The glucose binding scores for the 10 docked conformations obtained for the homologous proteins are shown in Table S5. The binding scores of the test proteins of a particular species were statistically compared with the binding scores of positive controls, negative controls, and in-between positive and negative controls, respectively, of the same species. This was repeated for the other species too. Then, binding scores of similar proteins from two different species but belonging to the same set were statistically compared. Statistical analyses were done through two-tailed Student's *t* test assuming equal variances. The p-values thus obtained are shown in Table S13b.

CONCLUSIONS

Glucose functions to stimulate and, consequently, increase insulin secretion. This process involves glucose-mediated glycolysis and ATP utilization as an energy source. However, within biological systems, cells can generate energy to a certain extent, prompting questions about the conservation of cellular energy. Recent research studies provide insights into how cells conserve energy and secrete specific proteins, often at the expense of other secretory proteins.[65] Notably, glucose molecules play a dual role: they not only contribute to energy generation through GLUT2-glucokinase-mediated phosphorylation in glycolysis but also enhance insulin secretion by binding to other proteins that facilitate glucose-mediated insulin secretion. Transcriptomic analyses of hyperglycemic-exposed-MIN6 cells identified upregulation of 3 secretion-specific genes corresponding to proteins KIF11, ATP6V0A4, and CACNB4. We have correlated the relevance of these 3 proteins with respect to cellular secretion and/or insulin secretion. Briefly, KIF11, also known as Kinesin-related motor protein Eg5, mediates secretory protein transport to the cell membrane from the Golgi complex through the transport of RAB6 containing CARTS[28] expanded as carriers of the trans-Golgi to the cell surface toward the cell membrane.[29] RAB6 is a marker for secretory vesicles and can regulate post-Golgi secretion.[77] RAB6 mediates insulin vesicle exocytosis and secretion.[78] RAB6 also controls targeting of constitutive secretory vesicles through microtubule protein motor Kinesin-1 to ELKS-rich sites in the cell membrane.[79] ELKS is present in pancreatic β-cells near insulin granules docked on the PM and silencing of ELKS expression reduced GSIS.[80] CACNB4, one of the $Ca_V\beta4$ auxiliary subunits, remains attached to the transmembrane $Ca_V\alpha1$ subunit, thereby making up the functional Ca_V voltage-dependent calcium

https://doi.org/10.1021/acsomega.3c09171
ACS Omega 2024, 9, 11755−11768

channel staged on the pancreatic β-cell membrane. These channels regulate β-cell insulin secretion.[30−33] Mutation at the a3 locus or loss of function of the a3 isoform of V-type ATPase dampened insulin secretion in the isolated islets of oc/oc mice, indicating that the protein participates in the exocytosis of insulin secretory vesicles.[34] Also, the a4 isoform of V-type ATPase has been found to be expressed in kidneys regulating acid−base equilibrium.[35] Thus, based on our transcriptome data, we proceeded with these 3 proteins only, which are also known to be involved in cellular secretion. These proteins might sequester intracellular but nonphosphorylated glucose and may take the center stage behind GSIS. Hence, using ADT, glucose was investigated as a possible ligand for the above 3 proteins. Glucose showed a higher binding score (in kcal/mol) among all metabolites and other hexoses ($C_6H_{12}0_6$'s) with all the 3 proteins. Further, the glucose-affinity or binding scores with the 3 proteins were also compared with the scores (in kcal/mol) for glucose as a ligand for positive controls, GCK and GLUT2, and along with negative controls, RPA1, KU70−80, POLA1, ACAA1A, and POLR1A. The binding scores of glucose molecules for KIF11, ATP6V0A4, and CACNB4 were found to be closer to positive controls with statistically significant scores compared to negative controls. Of course, future wet-laboratory work on the binding of glucose to purified KIF11, CACNB4, and ATP6V0A4 molecules would provide further validation to the results obtained here. In this context, "wet validation" may explicitly require a careful dissection of the results depending on the technique (e.g., in vitro (i) single-cell-based vs population cell cultures[85,86], (ii) types of cells, e.g., MIN6 vs primary islets etc., or in vivo) while considering specific intracellular conditions (e.g., compartmental/local pH[86] etc.) encountered in specific wet-experimental systems. Furthermore, intracellular energy transactions,[65,87] especially viewing the role of glucose molecules as intracellular ligands rather than as a source of metabolic energy, will also need to be carefully analyzed. The computational approaches utilized here do not consider such variables arising out of wet-experimental set ups. The above said, we report glucose sequestration ability OR regulation-by-glucose-binding of the three cellular secretion-related proteins for the first time, thereby presenting strong evidence relating to a possibly direct role of intracellular but unphosphorylated glucose molecules in GSIS. This opens a unique and novel perspective toward understanding the pathology of clinical conditions pertaining to exogenous-insulin-requiring diabetes, including (onset of) Type 1 Diabetes, at a cellular level.

MATERIALS AND METHODOLOGY

Chemicals. Dulbecco's modified Eagle's medium (DMEM), fetal bovine serum (FBS), Penstrep, and trypsin-EDTA were obtained from Gibco. Monosodium phosphate (NaH2PO4), Rat/Mouse (EZRMI-13K) Insulin ELISA Assay Kit, and ethanol were purchased from Merck. Magnesium chloride ($MgCl_2$), glucose, calcium chloride ($CaCl_2$), potassium chloride (KCl), HEPES, monopotassium phosphate (KH_2PO_4), sodium chloride (NaCl), dipotassium phosphate (K_2HPO_4), sodium bicarbonate ($NaHCO_3$), formaldehyde, 2-propanol, BSA, and Bradford were purchased from Himedia, India. Glucose oxidase, 4-aminoantipyrine *N*-ethyl-*N*-sulfopropyl-*M*-toluidine, horseradish peroxidase, disodium phosphate (Na_2HPO_4), and chloroform were purchased from Sigma, India. Trizol was obtained from Ambion Life Technology.

Cell Maintenance. MIN6 (Mouse Insulinoma 6) cells were obtained from NCCS (National Center for Cell Sciences, Pune). Cells were fed with DMEM containing 25 mM of glucose and 10% FBS with 1% Penstrep at 37 °C and 5% CO_2 as per literature.[26,27] For long-term experiments and maintenance of healthy cells, cells were supplemented with media every second day and split when necessary. Cells with passages below 30 were used for the experiments.

Glucose-Stimulated Insulin Secretion (GSIS) Assays on MIN6 Cells. Cells were seeded at a density of 1×10^6 cells per well and used at 75% confluency for the experiments. Cells were washed with Krebs Ringer Bicarbonate Buffer (KCl 4.7 mM, NaCl 119 mM, $MgSO_4$ 1.2 mM, KH_2PO_4 1.19 mM, $CaCl_2$ 2.5 mM, HEPES 10 mM, and $NaHCO_3$ 20 mM with 0.1% BSA) at pH 7.4 without glucose. Cells were treated with 2.8 mM glucose for 0.5 h and then stimulated at 25 mM glucose in KRBH for 1 h at 37 °C and 5% CO_2 as per protocol.[27,81] The supernatant was removed and centrifuged at 2500 rpm for 5 min and stored at −20 °C for insulin estimation using the Insulin ELISA EZRMI-13K kit. Normalization of secreted insulin was done using total cellular protein, which was estimated by Bradford assay using BSA protein as a standard. Experiments were performed in triplicates.

RNA Isolation and Transcriptome Study. Cells were treated as described above for transcriptome studies. RNA was isolated by the Trizol method according to the manufacturer's protocol. Cells were treated with 1 mL of Trizol and the cell pellet was homogenized two to three times. Next, 0.2 mL of chloroform was added and incubated for 5 min on ice. The microcentrifuge tube was inverted and mixed 10 times, and the samples were incubated again for 2−3 min on ice. The sample was centrifuged in microcentrifuge tubes at 14,000 rpm for 15 min at 4 °C. After centrifugation, 3 distinct layers were formed. The aqueous layer containing RNA was transferred to a new tube and 0.5 mL of 2-propanol was added. The tube was inverted and mixed 10 times, and the samples were incubated for 10 min at −20 °C. The tube was then centrifuged at 14,000 rpm for 15 min to pellet down the total RNA. Next, the supernatant was discarded and 1 mL of 75% ethanol was added. The sample was then air-dried and dissolved in RNase-free water. It was then stored at −80 °C for the RNA sequencing studies. The purity of RNA was checked by a Multiskan GO Spectrophotometer.

Transcriptome Study and Data Analysis. Transcriptome studies were performed by Agrigenome Lab Private Limited, Kerala, India. The quality and quantity of isolated RNA were checked using an Agilent Tapestation 2200 and Qubit 3.0 fluorimeter. After preparation of the sample library, the quality of library was checked using Agilent Tapestation 2200 and quantified using a Qubit 3.0 fluorimeter, and the validated libraries were sequenced on Illumina Hiseq X10 Platform for 2 × 150 bp length with 50 million reads. Since 30−40 million reads are sufficient to be technically precise in measuring differential gene expression,[82,83] we sequenced our cDNA libraries with 50 million reads to achieve sufficient technical precision. Differential expression analysis was done using Cuffdiff, and gene ontology analysis (biological process, molecular function, and cellular component) was done through the Uniprot database. Mapping to a reference genome is a crucial factor in evaluating the sample quality. The mapping

https://doi.org/10.1021/acsomega.3c09171
ACS Omega 2024, 9, 11755−11768

was done on HISAT2 taking reference genome GRCm38 of *M. musculus*.

Transcriptome results were analyzed and presented in terms of Fragments Per Kilobase of transcript per million mapped reads (FPKM). However, it was recently suggested that Transcripts Per Million (TPM) may be a more accurate way to compare transcriptomes across samples.[84] Conversion of TPM was done using the equation $\mathrm{TPM} = 10^6 \times \frac{\mathrm{FPKM}}{\sum(\mathrm{FPKM})}$. Differential gene expression was analyzed in terms of both FPKM and TPM, but the genes of interest were found to be upregulated in both cases. So, we chose FPKM to present our transcriptome results.

Selection of Protein Structures, Glucose Binding Analyses Using AutoDock Tools 4.2.6 (ADT), and Subsequent Visualization of the Docked Conformations through Discovery Studio 2021 (DS). The protein structures used for glucose binding studies have been mentioned in Table 2 under "Results and Discussion section". The exact methodology, various file formats, and pipeline used for glucose binding analyses through ADT and subsequent visualization through DS have been mentioned elaborately in "Docking pipeline" in Supporting Information. Briefly, the protein file (.pdb format) was opened in ADT and water molecules were deleted, followed by addition of polar hydrogens and Kollman charges. The ligand file (.pdb format) was then opened in ADT and after proper initialization, the respective ligand-protein complex was saved (.pdbqt format). The grid box size dimensions were set to size_x = 126, size_y = 126, and size_z = 126. The respective Autogrid parameter file was then saved (.gpf format) and after a successful run, an Autogrid log file (.glg format) was generated. Then, the docking parameter file (.dpf format) was generated using Lamarckian Genetic Algorithm. After a successful run, a docking log file (.dlg format) was generated that contained information on 10 binding scores (kcal/mol) of the corresponding 10 docked ligand binding poses with the respective protein. The.dlg file was saved (.pdbqt format) for further analyses in DS as a 2D protein−ligand interaction.

Calculation of Pearson's Correlation Coefficient. The binding energies (kcal/mol) and the number of interactions for the respective conformations within a single protein were noted. This was done for every other protein molecule used. Pearson's correlation coefficient (r) was calculated between the obtained binding energies (kcal/mol) and the number of interactions for the respective conformations within a single protein, and for every other protein molecule used.

Statistical Analyses. Two-tailed Student's t test assuming equal variances was performed using Microsoft Excel 2016 to calculate the statistical significance between the groups. The p-values <0.05 were considered as statistically significant.

■ ASSOCIATED CONTENT

Data Availability Statement

The data sets generated and/or analyzed during the current study are available in the Gene Expression Omnibus (GEO) repository (NCBI-GEO), Accession ID: GSE226652 (Token: sbcxuogopdmptin, https://www.ncbi.nlm.nih.gov/geo/query/acc.cgi?acc=GSE226652).

Supporting Information

The Supporting Information is available free of charge at https://pubs.acs.org/doi/10.1021/acsomega.3c09171.

Fold change in log 2 FPKM at HyG condition set at a threshold of +1.5 for upregulated protein-coding genes. *Kif11*, *Cacnb4* and *Atp6v0a4* is marked in bold, and Fold change in log 2 FPKM at HyG condition set at a threshold of −1.5 for downregulated protein-coding genes, respectively (Table S1a,b); expression of 154 genes involved in glycolysis, TCA cycle, and electron transport chain were found to be unaffected by EGC as seen by FPKM log2FC, corresponding numbers are indicated in parentheses (Table S2); highest binding scores (kcal/mol) obtained for every ligand used, the corresponding conformation is indicated in parentheses alongside highest binding scores obtained (Table S3); binding scores of the 10 docked conformations for every protein−ligand used (Table S3a−o); respective Ligand-Protein coordinates with X, Y, Z axes dimension points, spacing and X, Y, Z axes points of center grid box as chosen in AutoDock Tools 4.2.6 (Table S4a−o); glucose binding scores (kcal/mol) of 10 docked conformations of the homologous proteins (Table S5); respective conformations, number of interactions and glucose binding scores (kcal/mol) obtained for the test molecules (KIF11, CACNB4, ATP6V0A4) as shown in Table S6a,b; positive controls (human and mouse Glucokinase, human and mouse GLUT2) in Table S7; and negative controls (RPA1, KU70−80, POLR1A, ACAA1A) in Table S8a,b respectively, using AutoDock Tools (ADT) (Tables S6a,b, S7, and S8a,b); calculation of Pearson's correlation coefficient (Table S9); visualization of the binding propensity of D-glucose (Table S10); all the ligands used for binding studies have been shown with their respective PubChem CID's (Table S11); statistical analyses between binding scores (kcal/mol) showing p-values as obtained (Table S12); glucose binding scores of homologous proteins previously not used for binding analyses and subsequent statistical analyses between binding scores (kcal/mol) showing p-values as obtained (Table S13a,b); different insulin-secreting model systems obtained from different species used to study GSIS (Table S14); docking pipeline: Glucose binding analyses using AutoDock Tools 4.2.6 (ADT) and subsequent visualization of the docked conformations through Discovery Studio 2021 (DS). The exact methodology and pipeline used has been shown (PDF)

■ AUTHOR INFORMATION

Corresponding Author

Aditya Mittal − *Kusuma School of Biological Sciences, Indian Institute of Technology Delhi (IIT Delhi), New Delhi 110016, India; Supercomputing Facility for Bioinformatics and Computational Biology (SCFBio), IIT Delhi, New Delhi 110016, India;* orcid.org/0000-0002-4030-0951; Email: amittal@bioschool.iitd.ac.in

Authors

Firdos − *Kusuma School of Biological Sciences, Indian Institute of Technology Delhi (IIT Delhi), New Delhi 110016, India*

Tapabrata Pramanik − *Kusuma School of Biological Sciences, Indian Institute of Technology Delhi (IIT Delhi), New Delhi 110016, India*

https://doi.org/10.1021/acsomega.3c09171
ACS Omega 2024, 9, 11755−11768

Prachi Verma − *Kusuma School of Biological Sciences, Indian Institute of Technology Delhi (IIT Delhi), New Delhi 110016, India*

Complete contact information is available at: https://pubs.acs.org/10.1021/acsomega.3c09171

Author Contributions

[§]Firdos and T.P. contributed equally to this work.

Notes

The authors declare no competing financial interest.

■ ACKNOWLEDGMENTS

Firdos and T.P. are grateful to CSIR and GATE-MoE, respectively, for providing fellowship support, and to P.V. for the initial drafting of Table [1]. A.M. is grateful to Siddhant Mittal for sharing the clinical manifestations of Type 1 diabetes based on personal observations. A.M. is also grateful to Shweta Mittal and C. S. Dey for the informal discussions that encouraged him to initiate research on the cellular aspects related to Type 1 diabetes.

■ ABBREVIATIONS

GSIS:glucose-stimulated insulin secretion; EGC:extracellular glucose concentrations; MIN6:mouse insulinoma 6; ADT:AutoDock Tools; DS:Discovery Studio 2021; DM:diabetes mellitus

■ REFERENCES

(1) Sun, H.; Saeedi, P.; Karuranga, S.; Pinkepank, M.; Ogurtsova, K.; Duncan, B. B.; Stein, C.; Basit, A.; Chan, J. C. N.; Mbanya, J. C.; Pavkov, M. E.; Ramachandaran, A.; Wild, S. H.; James, S.; Herman, W. H.; Zhang, P.; Bommer, C.; Kuo, S.; Boyko, E. J.; Magliano, D. J. IDF Diabetes Atlas: Global, Regional and Country-Level Diabetes Prevalence Estimates for 2021 and Projections for 2045. *Diabetes Res. Clin. Pract.* **2022**, *183*, No. 109119, DOI: 10.1016/j.diabres.2021.109119.

(2) American Diabetes Association. Diagnosis and Classification of Diabetes Mellitus *Diabetes Care* 2014; Vol. *37* 1, pp S81−S90 DOI: 10.2337/dc14-S081.

(3) Leahy, J. L. Pathogenesis of Type 2 Diabetes Mellitus. *Arch. Med. Res.* **2005**, *36* (3), 197−209.

(4) Gallwitz, B.; Kazda, C.; Kraus, P.; Nicolay, C.; Schernthaner, G. Contribution of Insulin Deficiency and Insulin Resistance to the Development of Type 2 Diabetes: Nature of Early Stage Diabetes. *Acta Diabetol.* **2013**, *50* (1), 39−45.

(5) Marchetti, P.; Dotta, F.; Lauro, D.; Purrello, F. An Overview of Pancreatic Beta-Cell Defects in Human Type 2 Diabetes: Implications for Treatment. *Regul. Pept.* **2008**, *146* (1−3), 4−11.

(6) Butler, A. E.; Janson, J.; Bonner-Weir, S.; Ritzel, R.; Rizza, R. A.; Butler, P. C. Cell Deficit and Increased-Cell Apoptosis in Humans With Type 2 Diabetes. *Diabetes* **2003**, *52*, 102−110.

(7) Del Guerra, S.; Lupi, R.; Marselli, L.; Masini, M.; Bugliani, M.; Sbrana, S.; Torri, S.; Pollera, M.; Boggi, U.; Mosca, F.; Del Prato, S.; Marchetti, P. Functional and Molecular Defects of Pancreatic Islets in Human Type 2 Diabetes. *Diabetes* **2005**, *54*, 727−735, DOI: 10.2337/diabetes.54.3.727.

(8) Dokken, B. B. The Pathophysiology of Cardiovascular Disease and Diabetes: Beyond Blood Pressure and Lipids. *Diabetes Spectrum* **2008**, *21*, 160−165.

(9) American Diabetes Association. Diagnosis and Classification of Diabetes Mellitus *Diabetes Care* 2011; Vol. *34* 1, pp S62−S69 DOI: 10.2337/dc11-S062.

(10) Benninger, R. K. P.; Head, W. S.; Zhang, M.; Satin, L. S.; Piston, D. W. Gap Junctions and Other Mechanisms of Cell-Cell Communication Regulate Basal Insulin Secretion in the Pancreatic Islet. *J. Physiol.* **2011**, *589* (22), 5453−5466.

(11) German, M. S. Glucose Sensing in Pancreatic Islet Beta Cells: The Key Role of Glucokinase and the Glycolytic Intermediates. *Proc. Natl. Acad. Sci. U.S.A.* **1993**, *90*, 1781−1785.

(12) Liang, Y.; Najafi, H.; Smith, R. M.; Zimmerman, E. C.; Magnuson, M. A.; Tal, M.; Matschinsky, F. M. Concordant Glucose Induction of Glucokinase, Glucose Usage, and Glucose-Stimulated Insulin Release in Pancreatic Islets Maintained in Organ Culture. *Diabetes* **1992**, *41*, 792−806.

(13) De Vos, A.; Heimberg, H.; Quartier, E.; Huypens, P.; Bouwens, L.; Pipeleers, D.; Schuit, F. Human and Rat Beta Cells Differ in Glucose Transporter but Not in Glucokinase Gene Expression. *J. Clin. Invest.* **1995**, *96* (5), 2489−2495.

(14) Thorens, B.; Mueckler, M. Glucose Transporters in the 21st Century. *Am. J. Physiol.: Endocrinol. Metab.* **2010**, *298*, 141−145.

(15) Thorens, B. GLUT2, Glucose Sensing and Glucose Homeostasis. *Diabetologia* **2015**, *58* (2), 221−232.

(16) MacDonald, P. E.; Joseph, J. W.; Rorsman, P. Glucose-Sensing Mechanisms in Pancreatic β-Cells. *Philos. Trans. R. Soc., B* **2005**, *360* (1464), 2211−2225.

(17) Meglasson, M. D.; Matschinsky, F. M. Pancreatic Islet Glucose Metabolism and Regulation of Insulin Secretion. *Diabetes/Metab. Rev.* **1986**, *2* (3), 163−214.

(18) Matschinsky, F. M.; Ellerman, J. E. Metabolism of Glucose in the Islets of Langerhans. *J. Biol. Chem.* **1968**, *243* (10), 2730−2736.

(19) Gembal, M.; Gilon, P.; Henquin, J. C. Evidence That Glucose Can Control Insulin Release Independently from Its Action on ATP-Sensitive K+ Channels in Mouse B Cells. *J. Clin. Invest.* **1992**, *89* (4), 1288−1295.

(20) Henquin, J.-C. Perspectives in Diabetes Triggering and Amplifying Pathways of Regulation of Insulin Secretion by Glucose. *Diabetes* **2000**, *49*, 1751−1760.

(21) Prentki, M.; Matschinsky, F. M.; Madiraju, S. R. M. Metabolic Signaling in Fuel-Induced Insulin Secretion. *Cell Metab.* **2013**, *18* (2), 162−185.

(22) Seino, S.; Shibasaki, T.; Minami, K. Dynamics of Insulin Secretion and the Clinical Implications for Obesity and Diabetes. *J. Clin. Invest.* **2011**, *121* (6), 2118−2125.

(23) Tal, M.; Liang, Y.; Najafi, H.; Lodish, H. F.; Matschinsky, F. M. Expression and Function of GLUT-1 and GLUT-2 Glucose Transporter Isoforms in Cells of Cultured Rat Pancreatic Islets. *J. Biol. Chem.* **1992**, *267* (24), 17241−17247.

(24) Aronoff, S. L.; Berkowitz, K.; Shreiner, B.; Want, L. Glucose Metabolism and Regulation: Beyond Insulin and Glucagon. *Diabetes Spectrum* **2004**, *17* (3), 183−190, DOI: 10.2337/diaspect.17.3.183.

(25) Aamodt, K. I.; Powers, A. C. Signals in the Pancreatic Islet Microenvironment Influence β-Cell Proliferation. *Diabetes, Obes. Metab.* **2017**, *19*, 124−136.

(26) Miyazaki, J.-I.; Araki, K.; Yamato, E.; Ikegami, H.; Asano, T.; Shibasaki, Y.; Oka, Y.; Yamamura, K.-I. Establishment of a Pancreatic Beta Cell Line That Retains Glucose-Inducible Insulin Secretion: Special Reference to Expression of Glucose Transporter Isoforms. *Endocrinology* **1990**, *127* (1), 126−132.

(27) Ishihara, H.; Asano, T.; Tsukuda, K.; Katagiri, H.; Inukai, K.; Anai, M.; Kikuchi, M.; Yazaki, Y.; Miyazaki, J.-I.; Oka, Y. Pancreatic Beta Cell Line MIN6 Exhibits Characteristics of Glucose Metabolism and Glucose-Stimulated Insulin Secretion Similar to Those of Normal Islets. *Diabetologia* **1993**, *36*, 1139−1145.

(28) Wakana, Y.; Van Galen, J.; Meissner, F.; Scarpa, M.; Polishchuk, R. S.; Mann, M.; Malhotra, V. A New Class of Carriers That Transport Selective Cargo from the Trans Golgi Network to the Cell Surface. *EMBO J.* **2012**, *31* (20), 3976−3990.

(29) Wakana, Y.; Villeneuve, J.; van Galen, J.; Cruz-Garcia, D.; Tagaya, M.; Malhotra, V. Kinesin-5/Eg5 Is Important for Transport of CARTS from the Trans-Golgi Network to the Cell Surface. *J. Cell Biol.* **2013**, *202* (2), 241−250.

(30) Béguin, P.; Nagashima, K.; Gonoi, T.; Shibasaki, T.; Takahashi, K.; Kashima, Y.; Ozaki, N.; Geering, K.; Iwanaga, T.; Seino, S.

Regulation of Ca2+ Channel Expression at the Cell Surface by the Small G-Protein Kir/Gem. *Nature* **2001**, *411*, 701−706, DOI: 10.1038/35079621.
(31) Seino, S.; Chent, L.; Seino, M.; Blondel, O.; Takeda, J.; Johnson0, J. H.; Bell, G. I. Cloning of the A1 Subunit of a Voltage-Dependent Calcium Channel Expressed in Pancreatic Beta Cells. *Proc. Natl. Acad. Sci. U.S.A.* **1992**, *89*, 584−588, DOI: 10.1073/pnas.89.2.584.
(32) Ihara, Y.; Yamada, Y.; Fujii, Y.; Gonoi, T.; Yano, H.; Yasuda, K.; Inagaki, N.; Seino, Y.; Seino, S.; Kyoto, Y. Molecular Diversity and Functional Characterization of Voltage-Dependent Calcium Channels (CACN4) Expressed in Pancreatic Beta-Cells. *Mol. Endocrinol.* **1995**, *9*, 121−130.
(33) Yang, S. N.; Berggren, P. O. The Role of Voltage-Gated Calcium Channels in Pancreatic β-Cell Physiology and Pathophysiology. *Endocr. Rev.* **2006**, *27* (6), 621−676.
(34) Sun-wada, G. H.; Toyomura, T.; Murata, Y.; Yamamoto, A.; Futai, M.; Wada, Y. The A3 Isoform of V-ATPase Regulates Insulin Secretion from Pancreatic β-Cells. *J. Cell Sci.* **2006**, *119* (21), 4531−4540.
(35) Oka, T.; Murata, Y.; Namba, M.; Yoshimizu, T.; Toyomura, T.; Yamamoto, A.; Sun-Wada, G. H.; Hamasaki, N.; Wada, Y.; Futai, M. A4, a Unique Kidney-Specific Isoform of Mouse Vacuolar H + -ATPase Subunit a. *J. Biol. Chem.* **2001**, *276* (43), 40050−40054.
(36) Morris, G. M.; Goodsell, D. S.; Halliday, R. S.; Huey, R.; Hart, W. E.; Belew, R. K.; Olson, A. J. Automated Docking Using a Lamarckian Genetic Algorithm and an Empirical Binding Free Energy Function. *J. Comput. Chem.* **1639**, *19* (14), 1639−1662, DOI: 10.1002/(SICI)1096-987X(19981115)19:143.0.CO;2-B.
(37) Huey, R.; Morris, G. M.; Olson, A. J.; Goodsell, D. S. Software News and Update a Semiempirical Free Energy Force Field with Charge-Based Desolvation. *J. Comput. Chem.* **2007**, *28* (6), 1145−1152.
(38) Morris, G. M.; Ruth, H.; Lindstrom, W.; Sanner, M. F.; Belew, R. K.; Goodsell, D. S.; Olson, A. J. Software News and Updates AutoDock4 and AutoDockTools4: Automated Docking with Selective Receptor Flexibility. *J. Comput. Chem.* **2009**, *30* (16), 2785−2791.
(39) Dhorajiwala, T. M.; Halder, S. T.; Samant, L. Comparative in Silico Molecular Docking Analysis of L-Threonine-3-Dehydrogenase, a Protein Target against African Trypanosomiasis Using Selected Phytochemicals. *J. Appl. Biotechnol. Rep.* **2019**, *6* (3), 101−108.
(40) Nguyen, N. T.; Nguyen, T. H.; Pham, T. N. H.; Huy, N. T.; Van Bay, M.; Pham, M. Q.; Nam, P. C.; Vu, V. V.; Ngo, S. T. Autodock Vina Adopts More Accurate Binding Poses but Autodock4 Forms Better Binding Affinity. *J. Chem. Inf. Model.* **2020**, *60* (1), 204−211, DOI: 10.1021/acs.jcim.9b00778.
(41) Jumper, J.; Evans, R.; Pritzel, A.; Green, T.; Figurnov, M.; Ronneberger, O.; Tunyasuvunakool, K.; Bates, R.; Žídek, A.; Potapenko, A.; Bridgland, A.; Meyer, C.; Kohl, S. A. A.; Ballard, A. J.; Cowie, A.; Romera-Paredes, B.; Nikolov, S.; Jain, R.; Adler, J.; Back, T.; Petersen, S.; Reiman, D.; Clancy, E.; Zielinski, M.; Steinegger, M.; Pacholska, M.; Berghammer, T.; Bodenstein, S.; Silver, D.; Vinyals, O.; Senior, A. W.; Kavukcuoglu, K.; Kohli, P.; Hassabis, D. Highly Accurate Protein Structure Prediction with AlphaFold. *Nature* **2021**, *596* (7873), 583−589.
(42) Suzuki, A.; Nakauchi, H.; Taniguchi, H. Glucagon-like Peptide 1 (1−37) Converts Intestinal Epithelial Cells into Insulin-Producing Cells. *Proc. Natl. Acad. Sci. U.S.A.* **2003**, *100* (9), 5034−5039.
(43) Duan, F.; Curtis, K. L.; March, J. C. Secretion of Insulinotropic Proteins by Commensal Bacteria: Rewiring the Gut to Treat Diabetes. *Appl. Environ. Microbiol.* **2008**, *74* (23), 7437−7438.
(44) Santerre, R. F.; Cook, R. A.; Crisel, R. M. D.; Sharp, J. D.; Schmidt, R. J.; Williams, D. C.; Wilson, C. P. Insulin Synthesis in a Clonal Cell Line of Simian Virus 40-Transformed Hamster Pancreatic Beta Cells (Glucose Response/Bioassay/Receptor Assay/Acrylamide Gel Electrophoresis in NaDodSO4/Electron Microscopy). *Proc. Natl. Acad. Sci. U.S.A.* **1981**, *78* (7), 4339−4343.
(45) Asfari, M.; Janjic, D.; Meda, P.; Li, G.; Halban, P. A.; Wollheim, C. B. Establishment of 2-Mercaptoethanol-Dependent Differentiated Insulin-Secreting Cell Lines. *Endocrinology* **1992**, *130* (1), 167−178, DOI: 10.1210/endo.130.1.1370150.
(46) Hohmeier, H. E.; Mulder, H.; Chen, G.; Henkel-Rieger, R.; Prentki, M.; Newgard, C. B. Isolation of INS-1-Derived Cell Lines With Robust ATP-Sensitive K + Channel-Dependent and-Independent Glucose-Stimulated Insulin Secretion. *Diabetes* **2000**, *49*, 424−430, DOI: 10.2337/diabetes.49.3.424.
(47) Merglen, A.; Theander, S.; Rubi, B.; Chaffard, G.; Wollheim, C. B.; Maechler, P. Glucose Sensitivity and Metabolism-Secretion Coupling Studied during Two-Year Continuous Culture in INS-1E Insulinoma Cells. *Endocrinology* **2004**, *145* (2), 667−678.
(48) Mcclenaghan, N. H.; Barnett, C. R.; Ah-Sing, E.; Abdel-Wahab, Y. H. A.; O'harte, F. P. M.; Yoon, T.-W.; Swanston-Flatt, S. K.; Flatt, P. R. Characterization of a Novel Glucose-Responsive Insulin-Secreting Cell Line, BRIN-BD11, Produced by Electrofusion From the School of Biomedical Sciences. *Diabetes* **1996**, *45*, 1132−1140, DOI: 10.2337/diab.45.8.1132.
(49) Gazdar, A. F.; Chickt, W. L.; Oie, H. K.; Sims, H. L.; Kingt, D. L.; Weirt, G. C.; Laurist, V. Continuous, Clonal, Insulin-and Somatostatin-Secreting Cell Lines Established from a Transplantable Rat Islet Cell Tumor [Athymic Nude Mice/APUD (Amine-Handling) Cells/Insulinomal. *Proc. Natl. Acad. Sci. U.S.A.* **1980**, *77* (6), 3519−3523, DOI: 10.1073/pnas.77.6.3519.
(50) Praz, G. A.; Halban, P. A.; Wollheim, C. B.; Blondel, B.; Strauss, A. J.; Renold, A. E. Regulation of Immunoreactive-Insulin Release from a Rat Cell Line (RINm5F). *Biochem. J.* **1983**, *210*, 345−352.
(51) Carrington, C. A.; Rubery, E. D.; Pearson, E. C.; Hales, C. N. Five New Insulin-Producing Cell Lines with Differing Secretory Properties. *J. Endocrinol.* **1986**, *109*, 193−200.
(52) Efrat, S.; Lindet, S.; Kofodt, H.; Spector, D.; Delannoy, M.; Grant, S.; Hanahan, D.; Baekkeskovt, S. Beta-Cell Lines Derived from Transgenic Mice Expressing a Hybrid Insulin Gene Oncogene (Immortalization of Rare Cell Types/Insulin Secretion/Insulinoma Lines). *Proc. Natl. Acad. Sci. U.S.A.* **1988**, *85*, 9037−9041, DOI: 10.1073/pnas.85.23.9037.
(53) Poitout, V.; Stout, L. E.; Armstrong, M. B.; Walseth, T. F.; Sorenson, R. L.; Robertson, R. P. Morphological and Functional Characterization of Beta TC-6 Cells-an Insulin-Secreting Cell Line Derived From Transgenic Mice. *Diabetes* **1995**, *44*, 306−313.
(54) Hamaguchi, K.; Gaskins, H. R.; Leiter, E. H. NIT-1, a Pancreatic Beta-Cell Line Established From a Transgenic NOD/Lt Mouse. *Diabetes* **1991**, *40*, 842−849.
(55) Gilligan, A.; Jewett, L.; Simon, D.; Damjanov, I.; Matschinsky, F. M.; Weik, H.; Pinkert, C.; Knowles, B. B. Functional Pancreatic P-Cell Line From SV40 T-Antigen Transgenic Mouse. *Diabetes* **1989**, *38*, 1056−1062, DOI: 10.2337/diab.38.8.1056.
(56) Radvanyi, F.; Christgau, S.; Baekkeskov, S.; Jolicoeur, C.; Hanahan, D. Pancreatic Beta Cells Cultured from Individual Preneoplastic Foci in a Multistage Tumorigenesis Pathway: A Potentially General Technique for Isolating Physiologically Representative Cell Lines. *Mol. Cell. Biol.* **1993**, *13* (7), 4223−4232, DOI: 10.1128/MCB.13.7.4223.
(57) Ravassard, P.; Hazhouz, Y.; Pechberty, S.; Bricout-Neveu, E.; Armanet, M.; Czernichow, P.; Scharfmann, R. A Genetically Engineered Human Pancreatic β Cell Line Exhibiting Glucose-Inducible Insulin Secretion. *J. Clin. Invest.* **2011**, *121* (9), 3589−3597.
(58) Weir, G. C.; Bonner-Weir, S. Finally! A Human Pancreatic β Cell Line. *J. Clin. Invest.* **2011**, *121* (9), 3395−3397.
(59) de la Tour, D. D.; Halvorsen, T.; Demeterco, C.; rn Tyrberg, B.; Itkin-Ansari, P.; Loy, M.; Yoo, S.-J.; Hao, E.; Bossie, S.; Levine, F. Cell Differentiation from a Human Pancreatic Cell Line in Vitro and in Vivo. *Mol. Endocrinol.* **2001**, *15* (3), 476−483.
(60) Baroni, M. G.; Cavallo, M. G.; Mark, M.; Monetini, L.; Stoehrer, B.; Pozzilli, P. Beta-Cell Gene Expression and Functional Characterisation of the Human Insulinoma Cell Line CM. *J. Endocrinol.* **1999**, *161*, 59−68.
(61) Wang, S.; Beattie, G. M.; Mally, M. I.; Cirulli, V.; Itkin-Ansari, P.; Lopez, A. D.; Hayek, A.; Levine, F. Isolation and Characterization

https://doi.org/10.1021/acsomega.3c09171
ACS Omega 2024, 9, 11755−11768

of a Cell Line from the Epithelial Cells of the Human Fetal Pancreas. *Cell Transplant.* **1997**, *6* (1), 59−67.
(62) Narushima, M.; Kobayashi, N.; Okitsu, T.; Tanaka, Y.; Li, S. A.; Chen, Y.; Miki, A.; Tanaka, K.; Nakaji, S.; Takei, K.; Gutierrez, A. S.; Rivas-Carrillo, J. D.; Navarro-Álvarez, N.; Jun, H. S.; Westerman, K. A.; Noguchi, H.; Lakey, J. R. T.; Leboulch, P.; Tanaka, N.; Yoon, J. W. A Human β-Cell Line for Transplantation Therapy to Control Type 1 Diabetes. *Nat. Biotechnol.* **2005**, *23* (10), 1274−1282.
(63) Ashcroft, S. J. H.; Bassett, J. M.; Randle, P. J. Insulin Secretion Mechanisms and Glucose Metabolism in Isolated Islets. *Diabetes* **1972**, *21*, 538−545.
(64) Dai, C.; Brissova, M.; Hang, Y.; Thompson, C.; Poffenberger, G.; Shostak, A.; Chen, Z.; Stein, R.; Powers, A. C. Islet-Enriched Gene Expression and Glucose-Induced Insulin Secretion in Human and Mouse Islets. *Diabetologia* **2012**, *55* (3), 707−718.
(65) Firdos; Mittal, A. Secretory Conservation in Insulin Producing Cells: Is There a System-Level Law of Mass Action in Biology? *ACS Omega* **2023**, *8*, 37573−37583, DOI: 10.1021/acsomega.3c06058.
(66) Zaim, S. R.; Kenost, C.; Berghout, J.; Vitali, F.; Zhang, H. H.; Lussier, Y. A. Evaluating Single-Subject Study Methods for Personal Transcriptomic Interpretations to Advance Precision Medicine. *BMC Med. Genomics* **2019**, *12*, No. 96, DOI: 10.1186/s12920-019-0513-8.
(67) Kamata, K.; Mitsuya, M.; Nishimura, T.; Eiki, J. I.; Nagata, Y. Structural Basis for Allosteric Regulation of the Monomeric Allosteric Enzyme Human Glucokinase. *Structure* **2004**, *12* (3), 429−438.
(68) Bell, G. I.; Pilkis, S. J.; Weber, I. T.; Polonsky, K. S. Glucokinase Mutations, Insulin Secretion, and Diabetes Mellitus. *Annu. Rev. Physiol.* **1996**, *58*, 171−186.
(69) Molnes, J.; Bjørkhaug, L.; Søvik, O.; Njølstad, P. R.; Flatmark, T. Catalytic Activation of Human Glucokinase by Substrate Binding - Residue Contacts Involved in the Binding of D-Glucose to the Super-Open Form and Conformational Transitions. *FEBS J.* **2008**, *275* (10), 2467−2481.
(70) Yellapu, N. K.; Kandlapalli, K.; Valasani, K. R.; Sarma, P. V. G. K.; Matcha, B. Structural Variations of Human Glucokinase Glu256Lys in MODY2 Condition Using Molecular Dynamics Study. *Biotechnol. Res. Int.* **2013**, *2013*, No. 264793, DOI: 10.1155/2013/264793.
(71) Mueckler, M.; Thorens, B. The SLC2 (GLUT) Family of Membrane Transporters. *Mol. Aspects Med.* **2013**, *34* (2−3), 121−138.
(72) Johnson, J. H.; Newgard, C. B.; Milburn, J. L.; Lodish, H. F.; Thorens, B. The High Km Glucose Transporter of Islets of Langerhans Is Functionally Similar to the Low Affinity Transporter of Liver and Has an Identical Primary Sequence. *J. Biol. Chem.* **1990**, *265* (12), 6548−6551.
(73) Iynedjian, P. B. Molecular Physiology of Mammalian Glucokinase. *Cell. Mol. Life Sci.* **2009**, *66* (1), 27−42.
(74) Williams, T. F.; Exton, J. H.; Park, C. R.; Regen, D. M. Stereospecific Transport of Glucose in the Perfused Rat Liver. *Am. J. Physiol.-Legacy Content* **1968**, *215* (5), 1200−1209.
(75) Nomura, K.; Mikami, B.; Morita, Y. Interaction of Soybean Beta-Amylase with Glucose. *J. Biochem.* **1986**, *100* (5), 1175−1183.
(76) Antoine, M.; Boutin, J. A.; Ferry, G. Binding Kinetics of Glucose and Allosteric Activators to Human Glucokinase Reveal Multiple Conformational States. *Biochemistry* **2009**, *48* (23), 5466−5482.
(77) Fourriere, L.; Kasri, A.; Gareil, N.; Bardin, S.; Bousquet, H.; Pereira, D.; Perez, F.; Goud, B.; Boncompain, G.; Miserey-Lenkei, S. RAB6 and Microtubules Restrict Protein Secretion to Focal Adhesions. *J. Cell Biol.* **2019**, *218* (7), 2215−2231.
(78) Xiong, Q.-Y.; Yu, C.; Zhang, Y.; Ling, L.; Wang, L.; Gao, J.-L. Key Proteins Involved in Insulin Vesicle Exocytosis and Secretion. *Biomed. Rep.* **2017**, *6* (2), 134−139.
(79) Grigoriev, I.; Splinter, D.; Keijzer, N.; Wulf, P. S.; Demmers, J.; Ohtsuka, T.; Modesti, M.; Maly, I. V.; Grosveld, F.; Hoogenraad, C. C.; Akhmanova, A. Rab6 Regulates Transport and Targeting of Exocytotic Carriers. *Dev. Cell* **2007**, *13* (2), 305−314.
(80) Ohara-Imaizumi, M.; Ohtsuka, T.; Matsushima, S.; Akimoto, Y.; Nishiwaki, C.; Nakamichi, Y.; Kikuta, T.; Nagai, S.; Kawakami, H.; Watanabe, T.; Nagamatsu, S. ELKS, a Protein Structurally Related to the Active Zone-Associated Protein CAST, Is Expressed in Pancreatic Cells and Functions in Insulin Exocytosis: Interaction of ELKS with Exocytotic Machinery Analyzed by Total Internal Reflection Fluorescence Microscopy. *Mol. Biol. Cell* **2005**, *16*, 3289−3300.
(81) O'Driscoll, L.; Gammell, P.; Clynes, M. Mechanisms Associated with Loss of Glucose Responsiveness in Beta Cells. *Transplant. Proc.* **2004**, *36* (4), 1159−1162.
(82) Wang, Y.; Ghaffari, N.; Johnson, C. D.; Braga-Neto, U. M.; Wang, H.; Chen, R.; Zhou, H. Evaluation of the Coverage and Depth of Transcriptome by RNA-Seq in Chickens. *BMC Bioinf.* **2011**, *12*, No. S5, DOI: 10.1186/1471-2105-12-S10-S5.
(83) Hart, S. N.; Therneau, T. M.; Zhang, Y.; Poland, G. A.; Kocher, J. P. Calculating Sample Size Estimates for RNA Sequencing Data. *J. Comput. Biol.* **2013**, *20* (12), 970−978.
(84) Zhao, S.; Ye, Z.; Stanton, R. Misuse of RPKM or TPM Normalization When Comparing across Samples and Sequencing Protocols. *RNA* **2020**, *26* (8), 903−909, DOI: 10.1261/rna.074922.120.
(85) Mittal, A.; Leikina, E.; Bentz, J.; Chernomordik, L. V. Kinetics of influenza hemagglutinin-mediated membrane fusion as a function of technique. *Anal. Biochem.* **2002**, *303* (2), 145−152.
(86) Mittal, A.; Shangguan, T.; Bentz, J. Measuring pKa of activation and pKi of inactivation for influenza hemagglutinin from kinetics of membrane fusion of virions and of HA expressing cells. *Biophys. J.* **2002**, *83* (5), 2652−2666.
(87) Naresh, M.; Hasija, V.; Sharma, M.; Mittal, A. Synthesis of cellular organelles containing nano-magnets stunts growth of magnetotactic bacteria. *J. Nanosci. Nanotechnol.* **2010**, *10* (7), 4135−4144.

https://doi.org/10.1021/acsomega.3c09171
ACS Omega 2024, 9, 11755−11768

Supporting Information

(Re-)Viewing Role of Intracellular Glucose Beyond Extracellular Regulation of Glucose-Stimulated Insulin Secretion by Pancreatic cells

Firdos[1†], Tapabrata Pramanik[1†], Prachi Verma[1] and Aditya Mittal[1,2*]

[1]Kusuma School of Biological Sciences, Indian Institute of Technology Delhi (IIT Delhi), Hauz Khas, New Delhi 110016, India

[2]Supercomputing Facility for Bioinformatics and Computational Biology (SCFBio), IIT Delhi, Hauz Khas, New Delhi, 110016, India

†Equal Contribution

*Correspondence should be addressed to Aditya Mittal (email: amittal@bioschool.iitd.ac.in)

Table of Contents:

Supporting Information	Page Number
S1a	3-4
S1b	5-6
S2	7-9
S3 (S3a to S3o)	10-26
S4 (S4a to S4o)	27-53
S5	54
S6a, S6b	55-56
S7	56-57
S8a, S8b	58-59
S9	60
S10	61-63
S11	64
S12	65
S13a, S13b	66-68
S14	69-73
Docking pipeline	74-76

Table S1a: Fold change in log 2 FPKM at HyG condition set at a threshold of +1.5 for upregulated protein coding genes. *Kif11*, *Cacnb4* and *Atp6v0a4* is marked in bold.

Gene_ID	Gene	FPKM log2(fold change)
ENSMUSG00000063506	*Arhgap22*	17.41
ENSMUSG00000109523	*Gdf1*	9.06
ENSMUSG00000038600	***Atp6v0a4***	5.48
ENSMUSG00000078894	*2210418O10Rik*	5.35
ENSMUSG00000047810	*Ccdc88b*	5.01
ENSMUSG00000093954	*Gm16867*	4.97
ENSMUSG00000017412	***Cacnb4***	4.94
ENSMUSG00000079592	*C1qtnf5*	4.88
ENSMUSG00000073791	*Efcab7*	4.73
ENSMUSG00000038060	*Dlec1*	4.58
ENSMUSG00000026502	*Desi2*	4.43
ENSMUSG00000070806	*Zmynd12*	4.08
ENSMUSG00000053461	*Hhipl2*	3.49
ENSMUSG00000097239	*Gm27029*	3.40
ENSMUSG00000050944	*Efcab5*	3.28
ENSMUSG00000090015	*Gm15446*	3.28
ENSMUSG00000036168	*Ccdc38*	3.20
ENSMUSG00000012443	***Kif11***	3.05
ENSMUSG00000025330	*Padi4*	3.01
ENSMUSG00000027858	*Tspan2*	2.76
ENSMUSG00000113880	*A030005L19Rik*	2.76
ENSMUSG00000031519	*Asb5*	2.74
ENSMUSG00000078877	*Gm14295*	2.71
ENSMUSG00000019990	*Pde7b*	2.69
ENSMUSG00000041649	*Klf8*	2.66
ENSMUSG00000021768	*Dusp13*	2.66
ENSMUSG00000064036	*Mro*	2.61
ENSMUSG00000022102	*Dok2*	2.54
ENSMUSG00000026650	*Meig1*	2.53
ENSMUSG00000043629	*1700019D03Rik*	2.48
ENSMUSG00000069308	*Hist1h2bp*	2.47
ENSMUSG00000002107	*Celf2*	2.47
ENSMUSG00000002664	*Pspn*	2.43
ENSMUSG00000027505	*Fam209*	2.34
ENSMUSG00000041119	*Pde9a*	2.21
ENSMUSG00000073792	*Alg6*	2.19
ENSMUSG00000027338	*Prnd*	2.11
ENSMUSG00000062727	*H2bc12*	2.11
ENSMUSG00000063728	*Magea6*	2.11
ENSMUSG00000113786	*Gm49384*	2.09
ENSMUSG00000069266	*H4c2*	2.06
ENSMUSG00000026872	*Zeb2*	2.02
ENSMUSG00000059763	*Taar2*	2.00
ENSMUSG00000031410	*Nxf7*	1.97

ENSMUSG00000037708	*Spag6*	1.89
ENSMUSG00000032401	*Lctl*	1.88
ENSMUSG00000026500	*Cox20*	1.83
ENSMUSG00000027199	*Gatm*	1.83
ENSMUSG00000056305	*Usp39*	1.78
ENSMUSG00000070604	*Vsig10l*	1.78
ENSMUSG00000025758	*Plk4*	1.75
ENSMUSG00000092232	*Gm20521*	1.75
ENSMUSG00000041872	*Il17f*	1.74
ENSMUSG00000032000	*Birc3*	1.74
ENSMUSG00000096795	*Zfp433*	1.73
ENSMUSG00000022330	*Osr2*	1.72
ENSMUSG00000100200	*H2al1m*	1.71
ENSMUSG00000001020	*S100a4*	1.70
ENSMUSG00000117694	*Snhg4*	1.68
ENSMUSG00000095545	*Zfp969*	1.66
ENSMUSG00000081769	*Gm12216*	1.64
ENSMUSG00000110234	*Gm45799*	1.64
ENSMUSG00000025468	*Caly*	1.62
ENSMUSG00000037995	*Igsf9*	1.61
ENSMUSG00000028348	*Cavin4*	1.60
ENSMUSG00000039911	*Spsb1*	1.59
ENSMUSG00000018919	*Tm4sf5*	1.58
ENSMUSG00000034777	*Vax2*	1.58
ENSMUSG00000043807	*Ly6g5b*	1.56
ENSMUSG00000038057	*Dbil5*	1.56
ENSMUSG00000030966	*Trim21*	1.55
ENSMUSG00000051149	*Adnp*	1.54
ENSMUSG00000030345	*Dyrk4*	1.53
ENSMUSG00000041911	*Dlx1*	1.52
ENSMUSG00000010044	*Zmynd10*	1.50

Table S1b: Fold change in log 2 FPKM at HyG condition set at a threshold of -1.5 for downregulated protein coding genes.

gene_id	gene	FPKM log2(fold_change)
ENSMUSG00000078875	*Gm14419*	-6.20
ENSMUSG00000057969	*Sema3b*	-4.76
ENSMUSG00000078903	*Gm14391*	-4.74
ENSMUSG00000031618	*Nr3c2*	-4.67
ENSMUSG00000028339	*Col15a1*	-4.04
ENSMUSG00000000530	*Acvrl1*	-3.98
ENSMUSG00000078886	*Gm2026*	-3.96
ENSMUSG00000026637	*Traf5*	-3.75
ENSMUSG00000044217	*Aqp5*	-3.64
ENSMUSG00000032596	*Uba7*	-3.42
ENSMUSG00000020884	*Asgr1*	-3.24
ENSMUSG00000027500	*Stmn2*	-3.15
ENSMUSG00000054763	*Defb42*	-2.99
ENSMUSG00000114004	*Gm48552*	-2.91
ENSMUSG00000078880	*Gm14308*	-2.74
ENSMUSG00000089687	*Rab42*	-2.63
ENSMUSG00000020216	*Jsrp1*	-2.51
ENSMUSG00000100621	*Gm28374*	-2.49
ENSMUSG00000069300	*H2bc11*	-2.49
ENSMUSG00000025757	*Hspa4l*	-2.36
ENSMUSG00000028581	*Laptm5*	-2.33
ENSMUSG00000000411	*Tssk3*	-2.26
ENSMUSG00000020333	*Acsl6*	-2.20
ENSMUSG00000060803	*Gstp1*	-2.14
ENSMUSG00000045608	*Dbx2*	-2.14
ENSMUSG00000015950	*Ncf1*	-2.14
ENSMUSG00000003436	*Dll3*	-2.12
ENSMUSG00000030680	*Pagr1a*	-2.12
ENSMUSG00000028356	*Ambp*	-2.04
ENSMUSG00000039529	*Atp8b1*	-2.04
ENSMUSG00000040751	*Lat2*	-2.04
ENSMUSG00000001435	*Col18a1*	-2.01
ENSMUSG00000024824	*Rad9a*	-2.00
ENSMUSG00000021032	*Ngb*	-1.96
ENSMUSG00000069274	*H4c6*	-1.95
ENSMUSG00000027901	*Dennd2d*	-1.94
ENSMUSG00000101355	*H3c10*	-1.93
ENSMUSG00000020562	*Efcab10*	-1.93
ENSMUSG00000078588	*Ccdc24*	-1.91
ENSMUSG00000044916	*1700029I15Rik*	-1.88
ENSMUSG00000028141	*Oaz3*	-1.87
ENSMUSG00000069267	*H3c2*	-1.85
ENSMUSG00000069310	*H3c3*	-1.85
ENSMUSG00000024302	*Dtna*	-1.84
ENSMUSG00000049539	*H1f1*	-1.83

ENSMUSG00000053907	*Mat2a*	-1.82
ENSMUSG00000033149	*Phldb2*	-1.79
ENSMUSG00000058706	*0610030E20Rik*	-1.78
ENSMUSG00000028441	*1110017D15Rik*	-1.76
ENSMUSG00000101678	*Gm29609*	-1.76
ENSMUSG00000039115	*Itga9*	-1.76
ENSMUSG00000073427	*Gm4924*	-1.75
ENSMUSG00000023393	*Slc17a9*	-1.75
ENSMUSG00000021010	*Npas3*	-1.71
ENSMUSG00000078994	*Zfp429*	-1.71
ENSMUSG00000095742	*CAAA01147332.1*	-1.69
ENSMUSG00000074646	*6430550D23Rik*	-1.69
ENSMUSG00000057666	*Gapdh*	-1.68
ENSMUSG00000044034	*Npb*	-1.68
ENSMUSG00000069265	*H3c1*	-1.68
ENSMUSG00000078129	*Actl10*	-1.67
ENSMUSG00000070425	*Xntrpc*	-1.66
ENSMUSG00000002266	*Zim1*	-1.65
ENSMUSG00000045114	*Prrt2*	-1.58
ENSMUSG00000068323	*Slc4a5*	-1.58
ENSMUSG00000068686	*Cd59b*	-1.58
ENSMUSG00000095698	*Rhox2d*	-1.57
ENSMUSG00000052485	*Tmem171*	-1.57
ENSMUSG00000037692	*Ahdc1*	-1.56
ENSMUSG00000027684	*Mecom*	-1.56
ENSMUSG00000044556	*Tex38*	-1.56
ENSMUSG00000030790	*Adm*	-1.55
ENSMUSG00000109398	*Gm3854*	-1.55
ENSMUSG00000024391	*Apom*	-1.55
ENSMUSG00000055150	*Zfp78*	-1.53
ENSMUSG00000090093	*Gm14399*	-1.53
ENSMUSG00000001943	*Vsig2*	-1.53
ENSMUSG00000060798	*Intu*	-1.52

Table S2: Expression of 154 genes involved in glycolysis, TCA cycle, and electron transport chain were found to be unaffected by EGC as seen by FPKM log 2 FC, corresponding numbers are indicated in parentheses.

Gene	**FPKM log2 (fold_change)**	**Gene**	**FPKM log2 (fold_change)**
Glycolysis (13)		**Succinate dehydrogenase (ubiquinone) (4)**	
Slc2a1	0.129477	*Sdha*	-0.0212279
Slc2a2	0.478443	*Sdhb*	-0.0226989
Gck	-0.161379	*Sdhc*	0.356623
Gpi1	0.176844	*Sdhd*	0.0325765
Pfkl	0.1166	**Cytochrome bc1 complex (10)**	
Aldoa	0.103135	*Uqcrfs1*	0.0368768
Tpi1	0.00242379	*mt-Cytb*	-0.124625
Gapdh	-1.68012	*Cyc1*	0.159563
Pgk1	-0.0871155	*Uqcrc1*	0.574506
Pgam1	-0.0350487	*Uqcrc2*	-0.00128363
Pgam2	-0.539032	*Uqcrh*	-0.201539
Eno1	0.0340482	*Uqcrb*	0.00238799
Pkm	-0.00276637	*Uqcrq*	0.066611
Pyruvate oxidation (4)		*Uqcr10*	-0.259201
Pdha1	0.00705198	*Uqcr11*	-0.134678
Pdhb	0.0890469	**Cytochrome c oxidase (26)**	
Dlat	0.192814	*Cox10*	-0.212462
Dld	0.0637844	*mt-Co1*	-0.089138
TCA (14)		*mt-Co2*	-0.0103091
Cs	0.0617698	*mt-Co3*	0.0136884
Aco1	-0.0868456	*Cox4i1*	0.0407586
Aco2	0.131699	*Cox4i2*	0
Idh1	-0.0391724	*Cox5a*	0.0623172
Idh2	0.0544703	*Cox5b*	-0.134964
Ogdh	0.12405	*Cox6a1*	-0.124186
Suclg1	-0.040365	*Cox6a2*	0.499762
Suclg2	-0.557472	*Cox6b1*	-0.131535
Sucla2	0.0137215	*Cox6b2*	inf
Sdha	-0.0212279	*Cox6c*	-0.081579
Fh1	0.0195753	*Cox7a1*	-0.171086
Mdh1	0.117583	*Cox7a2*	-0.0349981
Mdh2	0.138587	*Cox7a2l*	-0.0494676
Pcx	0.0309434	*Cox7b*	-0.167232
NADH:ubiquinone oxidoreductase, mitochondria (7)		*Cox7b2*	inf
mt-Nd1	-0.119322	*Cox7c*	0.00544015
mt-Nd2	-0.234566	*Cox8a*	-0.171007

mt-Nd3	-0.179446	*Cox8b*	0
mt-Nd4	-0.182511	*Cox8c*	0
mt-Nd4l	-0.354229	*Cox11*	-0.410367
mt-Nd5	-0.454113	*Cox15*	0.335638
mt-Nd6	-0.376609	*Cox17*	-0.182519

NADH dehydrogenase (ubiquinone) Fe-S protein/flavoprotein complex, mitochondria (11)		*Cox20*	1.82773
Ndufs1	-0.00268643	**F-type ATPase (16)**	
Ndufs2	0.0247152	*Atp5a1*	-0.00506496
Ndufs3	0	*Atp5b*	-0.207685
Ndufs4	0.040037	*Atp5c1*	-0.0629166
Ndufs5	0.0222953	*Atp5d*	0.0666534
Ndufs6	-0.25042	*Atp5e*	0.0971921
Ndufs7	0.223296	*Atp5o*	-0.0989142
Ndufs8	-0.0426072	*mt-Atp6*	0.109196
Ndufv1	-0.0253616	*Atp5pb*	0.0448652
Ndufv2	-0.125322	*Atp5g1*	-0.171815
Ndufv3	-0.0714218	*Atp5g2*	-0.0486609
NADH dehydrogenase (ubiquinone) 1 alpha subcomplex (14)		*Atp5g3*	0.0116383
Ndufa1	0.0602351	*Atp5h*	-0.143714
Ndufa2	-0.0764759	*Atp5k*	0.110034
Ndufa3	-0.0667707	*Atp5j2*	-0.0615078
Ndufa4	-0.0148126	*Atp5j*	-0.057836
Ndufa5	0.0102769	*mt-Atp8*	-0.378299
Ndufa6	-0.0344079	**V-type ATPase (23)**	
Ndufa7	-0.0374823	*Atp6v1a*	-0.0461184
Ndufa8	0.0970221	*Atp6v1b1*	0
Ndufa9	-0.0191815	*Atp6v1c1*	-0.417038
Ndufa10	-0.00970045	*Atp6v1c2*	0
Ndufab1	-0.136161	*Atp6v1d*	0.00268642
Ndufa11	-0.168209	*Atp6v1e1*	0.0496172
Ndufa12	0.0617083	*Atp6v1e2*	inf
Ndufa13	-0.101487	*Atp6v1f*	0.0580141
NADH dehydrogenase (ubiquinone) 1 beta subcomplex (12)		*Atp6v1g1*	0.0263107
Ndufb2	-0.114007	*Atp6v1g2*	0.235369
Ndufb3	-0.113461	*Atp6v1g3*	0
Ndufb4	-0.178227	*Atp6v1h*	-0.0944612
Ndufb5	0.0778022	*Atp6v0a1*	0.183265
Ndufb6	0.0324454	*Atp6v0a4*	5.47832
Ndufb7	-0.117119	*Atp6v0a2*	0.0148742
Ndufb8	-0.0198604	*Tcirg1*	-0.048394
Ndufb9	-0.0305514	*Atp6v0b*	-0.0180279

Ndufb10	-0.0124879	*Atp6v0c*	0.169128
Ndufb11	-0.0242717	*Atp6v0d1*	0.14327
Ndufc1	0.31083	*Atp6v0d2*	0
Ndufc2	-0.0814358	*Atp6v0e*	-0.113659
		Atp6v0e2	0.121974
		Atp6ap1	-0.0341167

Table S3: Highest binding scores (kcal/mol) obtained for every ligand used, the corresponding conformation is indicated in parentheses alongside highest binding scores obtained.

Tables S3a to S3o: Binding scores of the 10 docked conformations for every protein-ligand used.

	Involved in glycolysis				Epimers of glucose		Other Aldohexoses					Other Ketohexoses			
	Glucose	G6P	F6P	F16BP	Mannose (C2)	Galactose (C4)	Altrose	Allose	Gulose	Idose	Talose	Fructose	Psicose	Tagatose	Sorbose
KIF11 mouse truncated	-4.62 (10)	-0.55 (3)	-0.84 (4)	+0.48 (10)	-1.42 (6)	-1.10 (9)	-1.48 (6)	-1.81 (9)	-2.47 (7)	-1.87 (5)	-1.36 (1)	-2.14 (9)	-1.54 (4)	-1.83 (4)	-1.63 (7)
KIF11 mouse (90-400)	-4.56 (9)	-3.71 (10)	-3.79 (2)	-1.73 (7)	-4.49 (1)	-3.39 (3)	-4.36 (1)	-4.71 (4)	-3.61 (8)	-4.24 (6)	-3.32 (7)	-3.76 (9)	-3.78 (2)	-3.82 (5)	-3.51 (1)
CACNB4 mouse truncated	-4.19 (6)	-1.51 (9)	-0.74 (9)	-0.49 (8)	-2.59 (8)	-2.36 (6)	-1.81 (2)	-3.33 (1)	-1.38 (6)	-1.70 (6)	-2.29 (7)	-1.49 (5)	-1.75 (9)	-2.60 (7)	-1.72 (6)
CACNB4 mouse (60-450)	-4.46 (3)	-3.26 (8)	-3.59 (10)	-0.37 (4)	-3.24 (2)	-4.00 (9)	-3.43 (7)	-3.02 (6)	-2.51 (5)	-2.99 (10)	-3.29 (1)	-2.47 (6)	-2.36 (7)	-2.25 (1)	-2.86 (10)
ATP6V0A4 mouse	-4.09 (1)	-2.04 (8)	-1.23 (1)	+0.01 (5)	-2.94 (3)	-1.68 (9)	-2.47 (9)	-2.67 (9)	-2.04 (9)	-2.16 (5)	-2.60 (6)	-2.81 (9)	-1.97 (3)	-2.45 (7)	-1.70 (1)
GCK human	-7.16 (1)	-3.49 (8)	-2.09 (5)	-0.34 (7)	-3.20 (2)	-3.03 (5)	-3.51 (10)	-4.13 (1)	-3.70 (1)	-3.29 (1)	-4.09 (8)	-3.36 (4)	-3.22 (10)	-3.09 (5)	-3.19 (3)
GCK mouse	-5.70 (4)	-3.63 (3)	-3.71 (10)	-1.92 (2)	-3.28 (9)	-3.88 (7)	-3.60 (5)	-2.96 (10)	-4.18 (7)	-3.25 (1)	-2.90 (8)	-3.35 (2)	-3.43 (1)	-3.28 (1)	-3.41 (1)
GLUT2 mouse	-5.35 (9)	-2.19 (10)	-2.88 (10)	-0.77 (2)	-4.00 (8)	-3.63 (10)	-3.89 (5)	-3.92 (9)	-2.67 (3)	-3.84 (1)	-2.86 (5)	-3.26 (8)	-3.73 (8)	-3.05 (1)	-3.49 (9)

GLUT2 human	-4.64 (3,4)	-2.25 (2)	-1.66 (8)	-1.36 (9)	-2.40 (1)	-4.05 (5)	-3.74 (5)	-3.77 (2)	-3.82 (10)	-3.33 (1)	-2.25 (4)	-3.66 (10)	-4.03 (9)	-3.58 (8)	-3.14 (5)
RPA1 human	-3.81 (4)	-1.95 (4)	-1.75 (2)	-0.74 (4)	-2.91 (4)	-3.53 (3)	-3.65 (3)	-3.00 (1)	-2.49 (6)	-3.60 (6)	-2.72 (9)	-2.47 (9)	-2.28 (4)	-2.48 (2)	-3.48 (10)
KU70-80 human	-3.75 (9)	-3.23 (6)	-2.93 (5)	-1.24 (10)	-4.48 (5)	-3.85 (9)	-3.78 (5)	-3.31 (10)	-4.41 (8)	-3.34 (2)	-3.60 (9)	-2.80 (9)	-4.47 (9)	-3.62 (5)	-3.42 (10)
POLA1 human	-3.58 (4)	-1.41 (4)	-1.26 (3)	+0.68 (3)	-3.42 (8)	-2.23 (4)	-3.19 (10)	-2.62 (7)	-2.00 (6)	-2.13 (6)	-2.52 (7)	-2.55 (10)	-2.49 (6)	-2.91 (9)	-2.53 (2)
ACAA1A mouse	-2.82 (1,3)	-2.50 (7)	-3.14 (3)	-2.67 (6)	-3.91 (10)	-2.93 (1)	-3.32 (6)	-3.48 (7)	-3.06 (3)	-3.88 (7)	-3.39 (6)	-3.43 (3)	-3.62 (3)	-3.60 (8)	-2.63 (6)
POLR1A human	-2.66 (7)	-1.31 (10)	-1.95 (6)	+0.41 (6)	-2.35 (8)	-2.17 (5)	-3.95 (4)	-2.47 (7)	-2.36 (9)	-1.93 (5)	-1.84 (6)	-2.68 (8)	-2.19 (5)	-2.84 (6)	-2.19 (4)

Table S3a: Binding scores (kcal/mol) of 10 docked conformations using Glucose as the ligand.

KIF11 mouse	-2.91	-2.91	-3.81	-2.18	-3.16	-3.8	-3.47	-2.08	-3.3	-4.62
tKIF11 (90-400) mouse	-3.51	-3.17	-3.15	-3.06	-2.94	-3	-2.49	-2.98	-4.56	-3.53
CACNB4 mouse	-3.37	-2.56	-2.72	-3.11	-3.87	-4.19	-3.79	-2.78	-3.17	-3.25
tCACNB4 (60-450) mouse	-3.43	-2.48	-4.46	-3.66	-2.54	-4.14	-3	-2.91	-2.71	-3.92
ATP6V0A4 mouse	-4.09	-3.53	-2.69	-2.69	-3.46	-2.98	-3.92	-3.71	-2.94	-2.39
GCK human	-7.16	-3.51	-3.4	-3.16	-2.9	-3.38	-3.28	-3.37	-2.93	-5.29
GCK mouse	-2.99	-4.99	-3.33	-5.7	-3.14	-2.94	-2.73	-3.14	-3.02	-2.51
GLUT2 mouse	-4.35	-3.22	-5.04	-4.18	-5.01	-3.32	-3.22	-3.04	-5.35	-5.23
GLUT2 human	-3.71	-3.5	-4.64	-4.64	-2.64	-4.22	-3.83	-3.41	-3.53	-3.74
RPA1 human	-3.81	-3.42	-3.28	-3.19	-2.67	-2.57	-2.29	-2.28	-2.26	-1.84
KU70-80 human	-2.46	-2.62	-1.81	-2.55	-2.42	-1.21	-1.98	-3.16	-3.75	-2.65
POLA1 human	-1.1	-2.2	-1.51	-3.58	-1.34	-2.11	-2.24	-3.47	-1.51	-2.32
ACAA1A mouse	-2.82	-1.95	-2.82	-2.55	-2.43	-1.62	-2.75	-2.16	-2.49	-2.63
POLR1A human	-2.66	-2.52	-2.31	-2.27	-2.05	-1.9	-1.6	-1.35	-1.05	-1.04

Table S3b: Binding scores (kcal/mol) of 10 docked conformations using G6P as the ligand.

KIF11 mouse	-0.55	-0.34	-0.33	-0.31	-0.27	-0.18	-0.17	0.23	0.53	0.94
tKIF11 (90-400) mouse	-3.71	-2.94	-2.82	-2.83	-2.34	-1.97	-1.85	-1.22	-1.2	-0.94
CACNB4 mouse	-1.51	-1.39	-1.23	-1.08	-1.07	-0.81	-0.76	-0.62	-0.48	0.16
tCACNB4 (60-450) mouse	-3.26	-2.96	-2.64	-2.37	-2.16	-1.96	-1.95	-1.85	-1.2	-1.2
ATP6V0A4 mouse	-2.04	-1.68	-1.47	-1.26	-0.92	-0.92	-0.49	-0.36	-0.25	0.04
GCK human	-3.49	-2.6	-2.5	-2.49	-2.37	-1.76	-1.63	-1.57	-1.39	-1.01
GCK mouse	-3.63	-2.86	-2.64	-2.27	-2.23	-1.77	-1.51	-1.5	-1.47	-1.17
GLUT2 mouse	-2.19	-2.06	-2	-1.87	-1.75	-1.74	-1.51	-1.42	-0.98	-0.8
GLUT2 human	-2.25	-2.02	-1.91	-1.83	-1.79	-1.73	-1.73	-1.6	-1.13	-0.78
RPA1 human	-1.95	-1.94	-1.9	-1.75	-1.75	-1.63	-1.16	-1.12	-1.07	-1.03
KU70-80 human	-3.23	-2.65	-2.6	-2.12	-1.63	-1.6	-1.45	-1.37	-1.35	-0.83
POLA1 human	-1.41	-1.26	-1.15	-1.03	-0.96	-0.9	-0.55	-0.47	-0.46	-0.37
ACAA1A mouse	-2.5	-2.23	-2.46	-2.35	-2.3	-2.2	-1.88	-1.63	-1.31	-0.78
POLR1A human	-1.31	-1.17	-1.17	-1.16	-0.67	-0.67	-0.21	-0.21	0.14	0.17

Table S3c: Binding scores (kcal/mol) of 10 docked conformations using F6P as the ligand.

KIF11 mouse	-0.84	-0.05	-0.02	0.06	0.27	0.32	0.56	0.64	0.81	1.21
tKIF11 (90-400) mouse	-3.79	-2.91	-2.26	-2.15	-1.88	-1.46	-1.06	-0.94	-0.58	-0.34
CACNB4 mouse	-0.74	-0.59	-0.31	-0.26	-0.17	0.19	0.2	0.45	0.47	0.53
tCACNB4 (60-450) mouse	-3.59	-3.14	-2.77	-1.67	-0.84	-0.43	-0.21	0.21	0.35	0.78
ATP6V0A4 mouse	-1.23	-1.12	-1.05	-0.29	-0.05	-0.02	0.4	0.65	0.79	1.02
GCK human	-2.09	-1.76	-1.61	-1.42	-1.34	-0.75	-0.62	-0.45	-0.39	0.22
GCK mouse	-3.71	-2.57	-2.26	-2.16	-1.53	-1.36	-1.18	-0.88	-0.81	0.36
GLUT2 mouse	-2.88	-2.22	-2.25	-1.71	-0.83	-0.72	-0.49	-0.3	0.07	0.4
GLUT2 human	-1.66	-0.5	-0.49	-0.36	-0.24	-0.06	0.57	0.81	0.89	0.93
RPA1 human	-1.75	-1.2	-0.97	-0.85	-0.83	-0.51	-0.36	-0.29	0.15	0.59
KU70-80 human	-2.93	-2.8	-2.66	-2.63	-1.64	-1.54	-1.35	-1.35	-0.47	-0.01
POLA1 human	-1.26	-0.76	-0.2	-0.2	-0.17	0.03	0.19	0.24	0.39	0.85
ACAA1A mouse	-3.14	-2.08	-2	-1.85	-1.8	-1.27	-1.25	-1.02	-0.82	-0.56
POLR1A human	-1.95	-1.4	-1.38	-1.13	-0.8	-0.25	0.04	0.07	0.19	0.24

Table S3d: Binding scores (kcal/mol) of 10 docked conformations using F16BP as the ligand.

KIF11 mouse	0.48	1.02	1.46	1.46	1.61	1.86	2.02	2.13	2.86	3.97
tKIF11 (90-400) mouse	-1.73	-1.03	-0.9	-0.47	0.04	0.12	0.21	0.87	1.09	1.69
CACNB4 mouse	-0.49	0.11	0.24	0.75	0.81	0.84	1.04	2.31	2.49	2.78
tCACNB4 (60-450) mouse	-0.37	-0.25	-0.04	0.22	0.45	0.46	0.94	1.02	1.43	1.65
ATP6V0A4 mouse	0.01	1.07	1.11	1.15	1.72	1.76	2.07	2.21	2.32	2.54
GCK human	-0.34	-0.29	-0.23	0.03	0.04	0.36	0.5	0.75	1.03	1.6
GCK mouse	-1.92	0.27	0.56	0.83	0.88	0.93	0.98	1.46	1.83	2.29
GLUT2 mouse	-0.77	-0.06	0.11	0.31	0.82	1.19	1.48	1.75	2.06	2.14
GLUT2 human	-1.36	-0.85	-0.7	-0.25	-0.07	0.36	0.7	1.21	2.14	2.26
RPA1 human	-0.74	-0.6	-0.15	-0.03	-0.02	0.01	0.51	0.69	1.31	1.72
KU70-80 human	-1.24	-0.63	-0.62	-0.48	-0.31	0.36	0.94	1.28	1.38	1.56
POLA1 human	0.68	0.85	1.12	1.18	1.97	1.99	2.07	2.21	2.19	2.69
ACAA1A mouse	-2.67	-2.02	-0.97	-0.57	-0.42	-0.29	-0.26	0.14	0.36	0.85
POLR1A human	0.41	0.59	0.75	0.8	0.99	1.21	1.55	1.76	2.11	2.17

Table S3e: Binding scores (kcal/mol) of 10 docked conformations using Mannose as the ligand.

KIF11 mouse	-1.42	-1.26	-1.25	-1.25	-1.06	-0.81	-0.72	-0.71	-0.65	-0.62
tKIF11 (90-400) mouse	-4.49	-4.27	-3.76	-3.53	-3.44	-3.16	-2.9	-2.69	-2.88	-2.65
CACNB4 mouse	-2.59	-2.09	-1.92	-1.73	-1.51	-1.33	-1.09	-1.05	-0.91	-0.8
tCACNB4 (60-450) mouse	-3.24	-3.16	-2.99	-2.39	-2	-1.95	-1.81	-1.77	-1.74	-1.34
ATP6V0A4 mouse	-2.94	-2.59	-2.46	-2.41	-2.23	-2.03	-2.03	-1.76	-1.72	-1.12
GCK human	-3.2	-3.16	-3.11	-2.93	-2.79	-2.43	-2.32	-2.26	-2.17	-2.13
GCK mouse	-3.28	-2.73	-2.57	-2.71	-2.61	-2.6	-2.55	-2.31	-2.09	-1.86
GLUT2 mouse	-4	-2.78	-2.68	-2.46	-2.27	-2.17	-2.09	-2.04	-1.91	-1.75
GLUT2 human	-2.4	-2.36	-2.18	-2.17	-2.08	-1.86	-1.86	-1.46	-1.3	-1.08
RPA1 human	-2.91	-2.86	-2.84	-2.35	-2.75	-2.5	-2.41	-2.4	-2.32	-2.08
KU70-80 human	-4.48	-4	-3.52	-2.43	-2.4	-2.24	-1.87	-1.8	-1.78	-1.7
POLA1 human	-3.42	-2.83	-2.79	-2.74	-1.72	-1.65	-1.56	-1.56	-1.36	-1.09
ACAA1A mouse	-3.91	-3.4	-2.2	-2.56	-2.52	-2.39	-1.83	-1.74	-1.69	-1.65
POLR1A human	-2.35	-2.25	-1.9	-1.81	-1.65	-1.58	-1.54	-1.53	-1.46	-1.28

Table S3f: Binding scores (kcal/mol) of 10 docked conformations using Galactose as the ligand.

KIF11 mouse	-1.1	-1.05	-0.95	-0.88	-0.86	-0.79	-0.71	-0.55	-0.47	-0.41
tKIF11 (90-400) mouse	-3.39	-3.35	-3.23	-2.95	-2.79	-2.85	-2.83	-2.42	-2.15	-2.12
CACNB4 mouse	-2.36	-2.04	-1.71	-1.4	-0.9	-0.83	-0.78	-0.68	-0.38	-0.26
tCACNB4 (60-450) mouse	-4	-3.42	-3.4	-3.31	-2.61	-2.55	-2.51	-2.54	-2.45	-2.42
ATP6V0A4 mouse	-1.68	-1.58	-1.44	-1.25	-1.19	-1.13	-1.18	-1.12	-0.98	-0.84
GCK human	-3.03	-2.94	-2.72	-2.54	-2.42	-2.2	-2.18	-1.76	-1.64	-1.49
GCK mouse	-3.88	-3.23	-2.88	-2.74	-2.67	-2.51	-2.37	-2.32	-2.17	-2.06
GLUT2 mouse	-3.63	-1.9	-3.23	-2.76	-3.12	-2.78	-2.58	-2.64	-2.06	-1.87
GLUT2 human	-4.05	-3.34	-2.3	-2.17	-2.17	-2.03	-1.94	-1.19	-1.09	-1.06
RPA1 human	-3.53	-3.29	-3	-2.53	-2.14	-2.1	-2.1	-1.86	-1.74	-1.2
KU70-80 human	-3.85	-3.68	-3.63	-2.75	-2.66	-2.43	-1.74	-1.71	-1.68	-1.29
POLA1 human	-2.23	-1.9	-1.79	-1.78	-1.77	-1.78	-1.72	-1.45	-1.29	-1.1
ACAA1A mouse	-2.93	-2.85	-2.35	-2.29	-2.27	-2.11	-2.26	-2.1	-1.74	-1.59
POLR1A human	-2.17	-1.89	-1.96	-1.58	-1.53	-1.52	-1.45	-0.9	-0.87	-0.72

Table S3g: Binding scores (kcal/mol) of 10 docked conformations using Altrose as the ligand.

KIF11 mouse	-1.48	-1.37	-1.3	-1.19	-1.05	-1.03	-1.03	-1	-0.95	-0.69
tKIF11 (90-400) mouse	-4.36	-3.93	-3.56	-3.43	-3.58	-3.35	-2.92	-2.85	-2.79	-2.43
CACNB4 mouse	-1.81	-1.64	-1.64	-1.6	-1.53	-1.46	-1.46	-1.35	-1.18	-1.14
tCACNB4 (60-450) mouse	-3.43	-2.94	-2.68	-3.29	-3.29	-2.82	-2.5	-2.05	-2.05	-1.55
ATP6V0A4 mouse	-2.47	-2.44	-2.32	-2.04	-1.86	-1.76	-1.42	-1.35	-1.34	-1.29
GCK human	-3.51	-3.03	-3.4	-3.03	-2.98	-2.92	-2.82	-2.58	-2.25	-2.34
GCK mouse	-3.6	-3.43	-2.81	-3.55	-3.54	-2.95	-2.56	-2.51	-2.35	-2.1
GLUT2 mouse	-3.89	-2.97	-2.92	-2.72	-2.68	-2.38	-2.34	-2.3	-2.04	-1.74
GLUT2 human	-3.74	-2.61	-3.1	-3.05	-3	-2.97	-2.87	-2.49	-2.48	-2.36
RPA1 human	-3.65	-3.26	-2.55	-2.87	-2.51	-2.39	-2.29	-2.28	-2.07	-1.95
KU70-80 human	-3.78	-3.64	-3.66	-2.64	-2.45	-2.28	-2.19	-2.08	-2.07	-2.06
POLA1 human	-3.19	-2.5	-2.12	-2.07	-1.98	-1.94	-1.94	-1.88	-1.84	-1.71
ACAA1A mouse	-3.32	-3.31	-3.28	-3.08	-2.94	-2.86	-2.81	-2.7	-2.59	-2.28
POLR1A human	-3.95	-2.27	-1.93	-1.88	-1.8	-1.79	-1.77	-1.63	-1.63	-1.27

Table S3h: Binding scores (kcal/mol) of 10 docked conformations using Allose as the ligand.

KIF11 mouse	-1.81	-1.69	-1.68	-1.62	-1.51	-1.47	-1.24	-1.21	-1.03	-0.88
tKIF11 (90-400) mouse	-4.71	-3.4	-3.75	-3.58	-2.93	-2.87	-2.78	-2.72	-2.68	-1.92
CACNB4 mouse	-3.33	-2.29	-2.12	-2.05	-2.01	-1.97	-1.8	-1.5	-1.41	-1.37
tCACNB4 (60-450) mouse	-3.02	-2.66	-2.05	-2.62	-2.54	-2.44	-1.93	-1.79	-1.66	-1.53
ATP6V0A4 mouse	-2.67	-2.39	-2.37	-2.06	-2.03	-2.01	-1.84	-1.47	-1.32	-1.2
GCK human	-4.13	-2.83	-3.15	-3.06	-2.88	-2.82	-2.82	-2.78	-2.52	-2.14
GCK mouse	-2.96	-2.86	-2.65	-2.58	-2.5	-2.45	-2.28	-2.23	-2	-1.99
GLUT2 mouse	-3.92	-2.98	-2.94	-3.3	-2.59	-2.24	-2.46	-2.29	-2.08	-1.94
GLUT2 human	-3.77	-3.4	-3.26	-2.75	-2.3	-1.93	-1.91	-1.89	-1.78	-1.56
RPA1 human	-3	-2.83	-2.63	-2.66	-2.4	-2.33	-2.29	-2.13	-2.17	-1.22
KU70-80 human	-3.31	-2.91	-3.28	-2.64	-2.57	-2.29	-2.16	-2.15	-1.93	-0.98
POLA1 human	-2.62	-2.44	-2.43	-2.4	-2.32	-2.28	-2.2	-1.74	-1.59	-1.27
ACAA1A mouse	-3.48	-2.49	-3.34	-2.39	-2.16	-2.14	-2.13	-1.8	-1.61	-1.26
POLR1A human	-2.47	-2.15	-2	-1.83	-1.74	-1.63	-1.42	-1.2	-1.14	-0.54

Table S3i: Binding scores (kcal/mol) of 10 docked conformations using Gulose as the ligand.

KIF11 mouse	-2.47	-1.74	-1.31	-1.05	-1.05	-0.81	-0.74	-0.38	-0.28	-0.19
tKIF11 (90-400) mouse	-3.61	-3.6	-3.28	-3.15	-3.02	-2.88	-2.36	-2.55	-2.22	-2.2
CACNB4 mouse	-1.38	-1.29	-1.12	-1.02	-0.98	-0.97	-0.86	-0.84	-0.7	-0.43
tCACNB4 (60-450) mouse	-2.51	-2.39	-2.36	-1.92	-1.89	-1.59	-1.5	-1.49	-1.26	-1.24
ATP6V0A4 mouse	-2.04	-1.69	-1.59	-1.29	-1.41	-1.05	-1.04	-1.04	-0.84	-0.76
GCK human	-3.7	-3.64	-3.34	-2.68	-2.66	-2.28	-2.25	-2.25	-2.12	-2.11
GCK mouse	-4.18	-3.11	-3.01	-2.5	-2.4	-2.37	-2.29	-2.26	-1.75	-1.69
GLUT2 mouse	-2.67	-2.65	-2.63	-2.28	-2.16	-2.42	-2.33	-2.27	-1.88	-1.78
GLUT2 human	-3.82	-2.6	-2.49	-2.47	-2.36	-2.23	-2.07	-2.02	-1.97	-1.93
RPA1 human	-2.49	-2.22	-2.32	-2.25	-2.15	-2.14	-2.14	-1.84	-1.56	-1.44
KU70-80 human	-4.41	-4.34	-3.58	-3.15	-2.95	-2.9	-2.3	-2.18	-1.74	-1.59
POLA1 human	-2	-1.85	-1.79	-1.74	-1.64	-1.59	-1.47	-1.36	-1.15	-1.12
ACAA1A mouse	-3.06	-2.69	-2.59	-2.54	-2.45	-2.4	-1.98	-1.9	-1.57	-1.41
POLR1A human	-2.36	-1.8	-1.58	-1.52	-1.51	-1.3	-1.25	-1.01	-0.82	-0.72

Table S3j: Binding scores (kcal/mol) of 10 docked conformations using Idose as the ligand.

KIF11 mouse	-1.87	-1.54	-1.5	-1.38	-1.33	-1.14	-0.86	-0.76	-0.68	-0.45
tKIF11 (90-400) mouse	-4.24	-3.79	-3.43	-3.26	-3.24	-3.14	-2.75	-3.34	-2.56	-2.32
CACNB4 mouse	-1.7	-1.7	-1.63	-1.53	-1.48	-1.45	-1.37	-1.37	-1.12	-0.93
tCACNB4 (60-450) mouse	-2.99	-2.52	-2.35	-2.23	-2.22	-2	-1.61	-1.57	-1.41	-1.06
ATP6V0A4 mouse	-2.16	-1.75	-1.92	-1.45	-1.35	-1.33	-1.18	-0.96	-0.93	-0.92
GCK human	-3.29	-3.19	-3.11	-3.01	-2.88	-2.62	-2.45	-1.96	-1.79	-1.68
GCK mouse	-3.25	-3.17	-3.13	-2.35	-2.34	-2.31	-1.8	-1.79	-1.66	-1.65
GLUT2 mouse	-3.84	-3.72	-3.1	-2.75	-2.39	-1.59	-2.29	-1.88	-1.79	-1.6
GLUT2 human	-3.33	-2.85	-2.54	-2.52	-2.49	-2.12	-1.98	-1.61	-1.42	-0.8
RPA1 human	-3.6	-3.43	-3.42	-2.92	-2.66	-2.37	-2.14	-1.95	-1.71	-1.36
KU70-80 human	-3.34	-3.28	-2.9	-2.36	-2.2	-1.83	-1.82	-1.72	-1.59	-1.49
POLA1 human	-2.13	-1.76	-1.6	-1.56	-1.54	-1.33	-1.32	-1.29	-1.15	-0.95
ACAA1A mouse	-3.88	-2.96	-2.46	-2.24	-2.1	-1.91	-1.81	-1.62	-1.46	-1.01
POLR1A human	-1.93	-1.82	-1.82	-1.77	-1.71	-1.7	-1.61	-1.31	-1.14	-0.57

Table S3k: Binding scores (kcal/mol) of 10 docked conformations using Talose as the ligand.

KIF11 mouse	-1.36	-1.27	-1.15	-0.97	-0.9	-0.87	-0.84	-0.61	-0.35	-0.25
tKIF11 (90-400) mouse	-3.32	-3.15	-3.01	-3.29	-2.92	-2.72	-2.7	-2.31	-2.21	-1.81
CACNB4 mouse	-2.29	-1.75	-1.59	-1.41	-1.35	-1.3	-1.29	-1.27	-1.12	-0.71
tCACNB4 (60-450) mouse	-3.29	-2.28	-1.84	-1.73	-1.46	-1.36	-1.31	-1.26	-1.18	-1
ATP6V0A4 mouse	-2.6	-1.96	-1.65	-1.66	-1.56	-1.46	-1.07	-1.04	-1.03	-0.71
GCK human	-4.09	-3.14	-2.61	-2.37	-2.17	-2.12	-2.03	-1.97	-1.67	-1.6
GCK mouse	-2.9	-2.55	-2.54	-2.4	-2.37	-2.32	-2.2	-2.11	-1.94	-1.72
GLUT2 mouse	-2.86	-2.85	-2.83	-2.67	-2.53	-2.48	-2.37	-2.17	-1.72	-1.44
GLUT2 human	-2.25	-2.03	-1.99	-1.91	-0.91	-1.89	-1.8	-1.54	-1.51	-1.12
RPA1 human	-2.72	-2.54	-2.03	-1.93	-1.85	-1.75	-1.68	-1.45	-1.43	-1.35
KU70-80 human	-3.6	-2.8	-3.59	-3.07	-2.85	-2.73	-2.27	-2.22	-2	-1.57
POLA1 human	-2.52	-2.11	-1.72	-1.66	-1.34	-1.33	-1.24	-1.17	-1.02	-0.77
ACAA1A mouse	-3.39	-3.3	-2.38	-2.35	-2.18	-2.18	-2.17	-2.05	-2.02	-1.86
POLR1A human	-1.84	-1.78	-1.68	-1.65	-1.47	-1.26	-1.18	-1.03	-0.82	-0.82

Table S3l: Binding scores (kcal/mol) of 10 docked conformations using Fructose as the ligand.

KIF11 mouse	-2.14	-1.6	-1.34	-1.08	-1.01	-0.92	-0.81	-0.79	-0.77	-0.61
tKIF11 (90-400) mouse	-3.76	-3.75	-3.6	-3.16	-2.96	-2.74	-2.52	-2.26	-2.12	-1.93
CACNB4 mouse	-1.49	-1.24	-1.19	-1.16	-1.11	-1.04	-1.01	-0.98	-0.88	-0.85
tCACNB4 (60-450) mouse	-2.47	-2.27	-2.01	-1.9	-1.74	-1.67	-1.49	-1.45	-1.4	-0.99
ATP6V0A4 mouse	-2.81	-2.69	-1.75	-1.69	-1.59	-1.57	-1.31	-1.25	-1.23	-0.98
GCK human	-3.36	-3.31	-2.87	-2.85	-2.69	-2.64	-2.64	-2.63	-1.86	-1.62
GCK mouse	-3.35	-3.31	-2.81	-3.04	-2.25	-2.68	-2.65	-2.18	-2.06	-1.45
GLUT2 mouse	-3.26	-3.13	-2.69	-2.87	-2.51	-2.43	-2.35	-2.41	-2.1	-1.56
GLUT2 human	-3.66	-2.78	-2.68	-2.68	-2.49	-2.35	-2.14	-1.67	-1.43	-0.87
RPA1 human	-2.47	-2.42	-2.15	-2.14	-2.13	-2.11	-2.04	-1.88	-1.77	-1.73
KU70-80 human	-2.8	-2.31	-2.3	-2.27	-2.07	-1.78	-1.72	-1.47	-1.37	-1.3
POLA1 human	-2.55	-2.38	-1.81	-1.75	-1.58	-1.55	-1.52	-1.17	-1.1	-1.03
ACAA1A mouse	-3.43	-2.68	-3.13	-2.62	-2.49	-2.28	-2.42	-2.22	-1.65	-1.43
POLR1A human	-2.68	-2.09	-1.99	-1.63	-1.54	-1.52	-1.32	-1.24	-1.15	-1.03

Table S3m: Binding scores (kcal/mol) of 10 docked conformations using Psicose as the ligand.

KIF11 mouse	-1.54	-1.35	-1.27	-1.2	-1.13	-1.05	-0.74	-0.61	-0.59	-0.32
tKIF11 (90-400) mouse	-3.78	-2.67	-3.63	-3.42	-3.14	-2.5	-1.93	-1.91	-1.7	-1.34
CACNB4 mouse	-1.75	-1.59	-1.55	-1.13	-1.11	-0.89	-0.89	-0.78	-0.72	-0.66
tCACNB4 (60-450) mouse	-2.36	-2.21	-2.19	-2.16	-1.52	-1.5	-1.21	-1.18	-1.1	-0.9
ATP6V0A4 mouse	-1.97	-1.79	-1.49	-1.36	-1.14	-1.04	-0.99	-0.44	-0.4	-0.36
GCK human	-3.22	-2.83	-2.75	-2.44	-2.21	-2.17	-2.07	-1.72	-1.52	-1.2
GCK mouse	-3.43	-2.7	-2.27	-2.16	-2.08	-2.12	-2	-1.72	-1.96	-1.94
GLUT2 mouse	-3.73	-3.41	-3.52	-3.37	-2.77	-2.47	-2.45	-1.83	-1.92	-1.82
GLUT2 human	-4.03	-3.49	-3.47	-2.65	-2.34	-1.44	-2.11	-1.7	-1.42	-1.15
RPA1 human	-2.28	-2.27	-1.87	-2.16	-2.13	-1.64	-1.62	-0.156	-1	-0.75
KU70-80 human	-4.47	-2.92	-2.78	-2.66	-2.5	-2.52	-2.46	-2.27	-1.92	-1.84
POLA1 human	-2.49	-2.47	-1.84	-1.78	-1.63	-1.31	-1.3	-1.24	-1.23	-0.88
ACAA1A mouse	-3.62	-3.04	-2.87	-2.02	-1.97	-1.86	-1.84	-1.77	-1.68	-1.38
POLR1A human	-2.19	-1.8	-1.78	-1.61	-1.74	-1.66	-1.57	-1.44	-1.23	-1.03

Table S3n: Binding scores (kcal/mol) of 10 docked conformations using Tagatose as the ligand.

KIF11 mouse	-1.83	-1.47	-1.36	-1.32	-1.06	-0.79	-0.79	-0.73	-0.73	-0.54
tKIF11 (90-400) mouse	-3.82	-3.59	-3.55	-3.51	-3.43	-3.08	-2.86	-2.65	-2.62	-2.48
CACNB4 mouse	-2.6	-1.76	-1.75	-1.71	-1.49	-1.47	-1.14	-1.14	-0.73	-0.52
tCACNB4 (60-450) mouse	-2.25	-1.8	-1.71	-1.69	-1.63	-1.42	-1.38	-1.13	-1.05	-0.91
ATP6V0A4 mouse	-2.45	-2.35	-1.58	-1.39	-1.37	-1.34	-1.2	-1.19	-0.65	-0.64
GCK human	-3.09	-2.87	-2.84	-2.78	-2.65	-2.64	-2.45	-2.37	-1.84	-1.62
GCK mouse	-3.28	-1.99	-3.23	-3.07	-2.86	-2.54	-2.37	-2.35	-2.07	-1.87
GLUT2 mouse	-3.05	-3	-2.85	-2.67	-2.61	-2.41	-2.18	-2.12	-1.8	-1.63
GLUT2 human	-3.58	-3.36	-2.59	-2.38	-2.41	-2.37	-2.13	-1.7	-1.59	-1.59
RPA1 human	-2.28	-2.21	-2.08	-2.08	-2.08	-1.86	-1.75	-1.73	-1.44	-1.35
KU70-80 human	-3.62	-2.89	-2.17	-2.02	-1.81	-1.57	-1.56	-1.54	-1.47	-1.28
POLA1 human	-2.91	-2.84	-2.7	-2.09	-1.97	-1.92	-1.82	-1.6	-1.34	-1.28
ACAA1A mouse	-3.6	-3.03	-2.64	-2.45	-2.36	-2.17	-2.06	-1.59	-1.54	-1.41
POLR1A human	-2.84	-2.71	-2.18	-2.01	-1.81	-1.57	-1.05	-1.49	-1.34	-1.31

Table S3o: Binding scores (kcal/mol) of 10 docked conformations using Sorbose as the ligand.

KIF11 mouse	-1.63	-1.4	-1.39	-1.35	-1.27	-1.21	-1.02	-0.97	-0.94	-0.91
tKIF11 (90-400) mouse	-3.51	-3.15	-2.76	-2.82	-2.79	-2.72	-1.86	-1.85	-1.62	-1.54
CACNB4 mouse	-1.72	-1.57	-1.51	-1.24	-1.17	-1.16	-1.16	-0.99	-0.73	-0.69
tCACNB4 (60-450) mouse	-2.86	-2.84	-1.9	-2.44	-2.17	-1.85	-1.51	-1.4	-1.33	-1.08
ATP6V0A4 mouse	-1.7	-1.69	-1.49	-1.29	-1.18	-0.97	-0.86	-0.81	-0.75	-0.62
GCK human	-3.19	-3.16	-2.89	-2.89	-2.8	-2.43	-2.14	-2.34	-2.25	-1.91
GCK mouse	-3.41	-3.41	-3.34	-2.99	-2.66	-2.61	-2.3	-2.33	-2.21	-2.06
GLUT2 mouse	-3.49	-3.18	-2.94	-2.75	-2.66	-2.61	-2.44	-2.21	-2.08	-1.98
GLUT2 human	-3.14	-2.19	-2.02	-2.05	-2.05	-1.83	-1.71	-1.51	-1.38	-1.3
RPA1 human	-3.48	-3.35	-3.16	-2.71	-2.46	-2.4	-2.38	-2.19	-1.99	-1.76
KU70-80 human	-3.42	-3.01	-2.64	-2.37	-2.32	-2.19	-2.06	-1.96	-1.59	-1.27
POLA1 human	-2.53	-2.49	2.39	-1.93	-1.91	-1.93	-1.82	-1.79	-1.1	-1.1
ACAA1A mouse	-2.63	-2.34	-2.31	-2.2	-2.09	-2.11	-1.91	-1.91	-1.64	-1.6
POLR1A human	-2.19	-1.93	-1.66	-1.66	-1.45	-1.39	-1.33	-1.26	-0.83	-0.63

Table S4: Respective Ligand-Protein co-ordinates with X, Y, Z axes dimension points, spacing and X, Y, Z axes points of centre grid box as chosen in AutoDock Tools 4.2.6.

Supplementary tables: S4a to S4o

Table S4a: KIF11 mouse and KIF11 human:

KIF11 mouse:

Ligand	X dimension	Y dimension	Z dimension	Spacing	X, Y, Z centre	Binding energy (kcal/mol)
Glucose	126	126	126	0.375	-7.221, 13.564, 6.179	-4.38
Glucose	126	108	126	0.442	8.656, 14.747, 12.125	-4.62
Psicose	126	126	126	1	26.884, 14.235, -12.521	-1.54
Talose	126	124	126	1	23.948, 13.202, -26.245	-1.36
Sorbose	126	126	126	1	21.581, 11.776, -21.286	-1.63
Tagatose	126	126	126	1	33.272, 8.099, -21.521	-1.83
Idose	126	126	126	1	22.617, 6.035, -25.860	-1.87
Gulose	126	126	126	1	17.198, 13.076, -11.493	-2.47
Allose	126	126	126	1	31.616, 1.592, -28.555	-1.81
Altrose	124	126	126	1	29.691, 1.840, -24.025	-1.48
Mannose	126	126	126	1	24.746, 0.592, -23.940	-1.42

Galactose	126	126	126	0.969	0.724, 10.697, -8.212	-1.1
F16BP	126	126	126	1	21.202, 16.927, -3.585	0.48
F6P	126	126	126	1	(1.295, -8.445, 4.657	-0.84
G6P	126	126	126	1	15.689, 24.138, 16.608	-0.55
Fructose	126	126	126	1	-11.447, -5.277, 10.639	-2.14

KIF11 human:

Ligand	X dimension	Y dimension	Z dimension	Spacing	X, Y, Z centre	Binding energy (kcal/mol)
Glucose	126	126	126	0.453	-16.669, 9.277, 8.891	-4.15

Table S4b: tKIF11 mouse (90-400) and tKIF11 human (90-400):

tKIF11 mouse (90-400):

Ligand	X dimension	Y dimension	Z dimension	Spacing	X, Y, Z centre	Binding energy (kcal/mol)
Glucose	126	126	126	0.458	-6.478, 10.954, -2.446	-4.56
Psicose	126	126	126	0.525	-10.474, 0.188, -4.351	-3.78
Talose	126	126	126	0.536	-3.663, 9.718, -4.232	-3.32
Sorbose	126	126	126	0.578	-8.139, 6.632, -3.838	-3.51
Tagatose	126	126	126	0.558	-8.357, 10.805, -3.385	-3.82
Idose	126	126	126	0.489	-6.599, 13.274, 5.247	-4.24
Gulose	126	126	126	0.508	-9.550, 13.339, -6.399	-3.61
Allose	126	126	126	0.506	-10.702, 4.295, -5.108	-4.71
Altrose	124	126	126	0.5	-8.571, 4.853, -3.634	-4.36
Mannose	126	126	126	0.444	-8.727, 9.626, 3.748	-4.49
Galactose	126	126	126	0.497	-10.278, 6.079, -6.415	-3.39
F16BP	126	126	126	0.503	-6.389, 10.824, -4.913	-1.73
F6P	126	126	126	0.503	-6.389, 10.824, -4.913	-3.79

G6P	126	126	126	0.506	-8.589, 12.799, -5.120	-3.71
Fructose	126	126	126	0.494	-7.708, 9.365, -4.153	-3.76

tKIF11 human (90-400):

Ligand	X dimension	Y dimension	Z dimension	Spacing	X, Y, Z centre	Binding energy (kcal/mol)
Glucose	126	126	126	0.458	-6.453, 10.945, 12.546	-4.31

Table S4c: CACNB4 mouse and CACNB4 human:

CACNB4 mouse: Ligand	X dimension	Y dimension	Z dimension	Spacing	X, Y, Z centre	Binding energy (kcal/mol)
Glucose	126	126	126	0.458	-6.478, 10.954, -2.446	-4.56
Psicose	126	126	126	0.967	-18.802, 3.702, 5.881	-1.75
Talose	126	124	126	0.917	-19.747, 4.644, 11.593	-2.29
Sorbose	126	126	126	1	-14.118, 8.941, 7.075	-1.72
Tagatose	126	126	126	0.961	-0.570, 2.818, 6.979	-2.6
Idose	126	126	126	0.806	-13.026, 0.448, 13.501	-1.7
Gulose	126	126	126	0.969	-12.883, 16.172, 12.068	-1.38
Allose	126	126	126	0.694	-8.804, 5.342, 6.751	-3.33
Altrose	124	126	126	0.828	-15.756, 8.007, 13.585	-1.81
Mannose	126	126	126	0.939	-12.982, 2.881, 8.060	-2.59
Galactose	126	126	126	0.969	-13.138, 4.673, 10.245	-2.36
F16BP	126	126	126	0.831	-7.355, 8.981, 4.388	-0.49
F6P	126	126	126	0.836	-15.622, -6.971, 7.663	-0.74
G6P	126	126	126	0.914	-8.049, 10.418, 11.443	-1.51
Fructose	126	126	126	0.919	-11.447, -5.277, 10.639	-1.49

CACNB4 human:

Ligand	X dimension	Y dimension	Z dimension	Spacing	X, Y, Z centre	Binding energy (kcal/mol)
Glucose	126	126	125	0.453	-16.669, 9.277, 8.891	-4.39

Table S4d: tCACNB4 mouse (60-450) and tCACNB4 human (60-450):

tCACNB4 mouse (60-450):

Ligand	X dimension	Y dimension	Z dimension	Spacing	X, Y, Z centre	Binding energy (kcal/mol)
Glucose	126	126	126	0.514	-10.479, 3.684, 5.567	-4.46
Psicose	126	126	126	0.764	-25.522, -2.295, -6.352	-2.36
Talose	126	126	126	0.747	-20.382, -7.380, 10.016	-3.29
Sorbose	126	126	126	0.733	-24.396, -8.477, 8.438	-2.86
Tagatose	126	126	126	0.886	-30.005, 10.358, 1.644	-2.25
Idose	126	126	126	0.733	-21.758, -7.033, 6.777	-2.99
Gulose	126	126	126	0.764	-28.583, 1.575, 12.068	-2.51
Allose	126	126	126	0.661	-11.346, -0.761, 1.312	-3.02
Altrose	124	126	126	0.606	-7.190, 2.931, 4.755	-3.43
Mannose	126	126	126	0.672	-9.858, -15.365, 7.839	-3.24
Galactose	126	126	126	0.497	-6.919, -0.426, 2.416	-4
F16BP	126	126	126	0.589	-9.715, -7.227, -1.116	-0.37
F6P	126	126	126	0.669	-10.975, 10.824, 10.004	-3.59
G6P	126	126	126	0.583	-13.510, -15.078, 2.322	-3.26

Fructose	126	126	126	0.678	-17.267, -11.222, 4.748	-2.47

tCACNB4 human (60-450):

Ligand	X dimension	Y dimension	Z dimension	Spacing	X, Y, Z centre	Binding energy (kcal/mol)
Glucose	126	126	126	0.375	-10.478, 3.557, 5.593	-4.52

Table S4e: ATP6V0A4 mouse and ATP6V0A4 human:

ATP6V0A4 mouse:

Ligand	X dimension	Y dimension	Z dimension	Spacing	X, Y, Z centre	Binding energy (kcal/mol)
Glucose	126	126	126	0.453	-2.936, 5.962, 0.058	-4.09
Psicose	126	126	126	1	-1.711, 3.896, 12.772	-1.97
Talose	126	124	126	1	3.692, 0.729, 12.872	-2.6
Sorbose	126	126	126	1	-8.049, 1.659, 8.085	-1.7
Tagatose	126	126	126	1	-0.570, 2.818, 6.979	-2.45
Idose	126	126	126	0.961	-8.917, -3.112, 6.777	-2.16
Gulose	126	126	126	1	-6.348, -0.682, 9.503	-2.04
Allose	126	126	126	0.956	-6.503, 3.343, 7.304	-2.67
Altrose	124	126	126	0.917	-12.061, -14.546, 9.911	-2.47
Mannose	126	126	126	0.889	-7.153, -8.523, 7.839	-2.94
Galactose	126	126	126	0.969	-13.138, 4.673, 10.245	-1.68
F16BP	126	126	126	0.831	-7.355, -0.187, 4.751	0.01
F6P	126	126	126	0.864	-10.037, -5.805, 4.135	-1.23
G6P	126	126	126	0.914	-8.049, -1.522, 12.729	-2.04

Fructose	126	126	126	0.892	-7.552, -3.218, 10.059	-2.81

ATP6V0A4 human:

Ligand	X dimension	Y dimension	Z dimension	Spacing	X, Y, Z centre	Binding energy (kcal/mol)
Glucose	126	126	126	0.453	-2.922, 5.988, 0.063	-4.22

Table S4f: GCK mouse:

Ligand	X dimension	Y dimension	Z dimension	Spacing	X, Y, Z centre	Binding energy (kcal/mol)
Glucose	126	126	126	0.375	0.572, 2.701, 0.112	-5.7
Psicose	126	126	126	0.558	0.595, 3.246, -7.608	-3.43
Talose	126	126	126	0.547	1.894, 8.338, -7.877	-2.9
Sorbose	126	126	126	0.581	-0.449, 7.915, -8.430	-3.41
Tagatose	126	126	126	0.553	2.141, 8.880, -7.375	-3.28
Idose	126	126	126	0.538	5.704, 0.884, -7.790	-3.25
Gulose	126	126	126	0.536	0.151, 3.526, -7.818	-4.18
Allose	126	126	126	0.55	-0.589, 0.098, -8.243	-2.96
Altrose	126	126	126	0.522	1.569, -1.176, -7.784	-3.6
Mannose	126	126	126	0.583	1.885, 3.736, -8.894	-3.28
Galactose	126	126	126	0.503	-0.107, 4.905, -7.252	-3.88
F16BP	126	126	126	0.519	-2.092, 2.505, -7.203	-1.92
F6P	126	126	126	0.475	1.512, 7.579, -6.801	-3.71
G6P	126	126	126	0.5	-6.009, 4.870, -7.573	-3.63
Fructose	126	126	126	0.517	2.066, 6.526, -6.823	-3.35

Table S4g: GCK human:

Ligand	X dimension	Y dimension	Z dimension	Spacing	X, Y, Z centre	Binding energy (kcal/mol)
Glucose	40	40	40	0.375	-0.033, 0.220, 0.946	-4
Glucose	126	126	126	0.375	27.896 2.222 71.382	-7.16
Psicose	126	126	126	0.531	2.757, 0.188, -0.764	-3.22
Talose	126	126	126	0.547	1.894, 5.867, 0.097	-4.09
Sorbose	126	126	126	0.536	5.081, 7.915, 0.179	-3.19
Tagatose	126	126	126	0.553	4.144, 8.520, 0.136	-3.09
Idose	126	126	126	0.532	5.704, 3.022, 0.082	-3.29
Gulose	126	126	126	0.525	1.734, 7.246, -0.796	-3.7
Allose	126	126	126	0.517	3.388, 3.602, -1.458	-4.13
Altrose	124	126	126	0.506	7.161, -0.013, 2.532	-3.51
Mannose	126	126	126	0.544	3.908, 3.430, 0.046	-3.2
Galactose	126	126	126	0.531	4.346, -3.315, 2.431	-3.03
F16BP	126	126	126	0.567	4.332, -8.784, 3.569	-0.34
F6P	126	126	126	0.536	5.408, 12.233, -2.102	-2.09
G6P	126	126	126	0.494	3.454, -0.684, 0.844	-3.49

Fructose	126	126	126	0.511	5.071, 5.531, 3.498	-3.36

Table S4h: GLUT2 mouse:

Ligand	X dimension	Y dimension	Z dimension	Spacing	X, Y, Z centre	Binding energy (kcal/mol)
Glucose	100	106	78	0.375	1.137, 1.433, 7.218	-5.35
Psicose	126	126	126	0.558	0.595, 7.278, 10.447	-3.73
Talose	126	126	126	0.575	-3.663, 9.718, 9.308	-2.86
Sorbose	126	126	126	0.622	-1.185, 6.632, 9.558	-3.49
Tagatose	126	126	126	0.647	2.141, 8.880, 10.489	-3.05
Idose	126	126	126	0.588	-3.585, 7.298, 9.793	-3.84
Gulose	126	126	126	0.597	-1.405, 4.326, 9.395	-2.67
Allose	126	126	126	0.622	-0.589, 0.098, 7.759	-3.92
Altrose	126	126	126	0.572	1.714, 5.988, 9.040	-3.89
Mannose	126	126	126	0.606	2.552, 7.793, 9.962	-4

Galactose	126	126	126	0.569	-0.659, 7.267, 7.827	-3.63
F16BP	126	126	126	0.564	0.520, 10.033, 13.293	-0.77
F6P	126	126	126	0.525	1.148, -2.065, 6.038	-2.88
G6P	126	126	126	0.578	-2.397, 4.032, 10.031	-2.19
Fructose	126	126	126	0.594	-1.405, 8.268, 10.674	-3.26

Table S4i : GLUT2 human:

Ligand	X dimension	Y dimension	Z dimension	Spacing	X, Y, Z centre	Binding energy (kcal/mol)
Glucose	126	94	126	0.375	-1.529, 1.420, 4.403	-4.64
Psicose	126	126	126	0.664	6.406, -8.753, 8.904	-4.03
Talose	126	126	126	0.731	6.997, 8.511, 0.097	-2.25
Sorbose	126	126	126	0.764	8.443, 15.719, 11.710	-3.14
Tagatose	126	126	126	0.697	6.890, 8.520, 0.136	-3.58
Idose	126	126	126	0.716	5.375, 6.219, -4.749	-3.33
Gulose	126	126	126	0.658	7.222, 7.246, 7.721	-3.82
Allose	126	126	126	0.661	5.280, 5.577, 4.572	-3.77
Altrose	124	126	126	0.611	6.341, -1.176, 1.739	-3.74
Mannose	126	126	126	0.628	3.474, -8.195, 1.952	-2.4
Galactose	126	126	126	0.625	-1.235, -3.483, 5.939	-4.05
F16BP	126	126	126	0.544	4.332, -8.784, 3.569	-1.36

F6P	126	126	126	0.664	2.330, 11.737, 9.393	-1.66
G6P	126	126	126	0.583	1.379, -15.078, 2.322	-2.25
Fructose	126	126	126	0.594	11.522, 7.854, 3.843	-3.66

Table S4j: RPA1 human:

Ligand	X dimension	Y dimension	Z dimension	Spacing	X, Y, Z centre	Binding energy (kcal/mol)
Glucose	126	126	126	0.639	-9.747, -5.247, -0.251	-3.81
Psicose	126	126	126	0.725	-3.499, 9.329, -4.800	-2.28
Talose	126	126	126	0.731	-1.193, 9.762, 0.097	-2.72
Sorbose	126	126	126	0.686	-10.012, 18.252, -5.728	-3.48
Tagatose	126	126	126	0.708	-4.346, 14.604, -3.834	-2.48
Idose	126	126	126	0.721	-3.919, 23.349, -3.058	-3.6
Gulose	126	126	126	0.733	-3.676, 9.897, -6.881	-2.49
Allose	126	126	126	0.667	-8.509, 22.953, -5.706	-3
Altrose	126	126	126	0.653	-7.908, -9.388, -3.458	-3.65
Mannose	126	126	126	0.644	-7.984, -6.778, -4.438	-2.91
Galactose	126	126	126	0.639	-7.456, -5.498, -1.212	-3.53
F16BP	126	126	126	0.638	-10.224, -11.705, 3.164	-0.74

F6P	126	126	126	0.703	-6.938, 6.261, -7.578	-1.75
G6P	126	126	126	0.639	-1.436, -3.030, -4.930	-1.95
Fructose	126	126	126	0.619	-1.385, 6.859, -0.227	-2.47

Table S4k: POLR1A human:

Ligand	X dimension	Y dimension	Z dimension	Spacing	X, Y, Z centre	Binding energy (kcal/mol)
Glucose	126	126	126	0.9	-11.991, -5.247, -0.251	-2.66
Psicose	126	126	126	0.875	-14.022, 0.889, -7.767	-2.19
Talose	126	126	126	0.931	-16.869, 8.658, 1.866	-1.84
Sorbose	126	126	126	0.942	-16.806, -7.491, -0.029	-2.19
Tagatose	126	126	126	0.931	-17.455, -4.789, -3.850	-2.84
Idose	126	126	126	0.892	-13.082, -6.149, -2.110	-1.93
Gulose	126	126	126	0.944	-13.180, -4.655, 11.681	-2.36
Allose	126	126	126	0.944	-13.180, -4.655, 11.681	-2.47
Altrose	126	126	126	0.869	-14.695, -9.388, -3.458	-3.95
Mannose	126	126	126	0.942	-14.998, -3.584, 0.033	-2.35
Galactose	126	126	126	0.917	-10.739, -8.475, -5.438	-2.17

F16BP	126	126	126	0.882	-15.507, -4.037, -0.228	0.41
F6P	126	126	126	0.825	-11.653, -7.243, -3.112	-1.95
G6P	126	126	126	0.883	-11.513, -2.695, -3.538	-1.31
Fructose	126	126	126	0.858	-10.027, -2.289, 2.828	-2.68

Table S4l: KU70-80 human:

Ligand	X dimension	Y dimension	Z dimension	Spacing	X, Y, Z centre	Binding energy (kcal/mol)
Glucose	126	126	126	0.847	13.055, -5.884, 123.367	-3.75
Psicose	126	126	126	0.814	15.380, -8.753, 116.674	-4.47
Talose	126	126	126	0.686	15.581, 8.658, 115.901	-3.6
Sorbose	126	126	126	0.792	9.969, -6.666, 113.522	-3.42
Tagatose	126	126	126	0.892	11.291, -6.058, 106.757	-3.62
Idose	126	126	126	0.866	14.363, -8.378, 111.866	-3.34
Gulose	126	126	126	0.664	15.641, 7.246, 121.288	-4.41
Allose	126	126	126	0.836	17.559, -9.406, 121.922	-3.31
Altrose	126	126	126	0.781	17.853, -6.946, 117.422	-3.78
Mannose	126	126	126	0.792	14.108, -6.138, 123.366	-4.48
Galactose	126	126	126	0.7	13.102, 2.913, 122.537	-3.85
F16BP	126	126	126	0.799	11.592, -10.819, 113.897	-1.24

F6P	126	126	126	0.769	15.304, -7.289, 125.418	-2.93
G6P	126	126	126	0.742	13.634, -6.837, 121.946	-3.23
Fructose	126	126	126	0.781	7.984, -5.302, 118.621	-2.8

Table S4m: KU70 mouse and KU70 human; KU80 mouse and KU80 human:

KU70 mouse:

Ligand	X dimension	Y dimension	Z dimension	Spacing	X, Y, Z centre	Binding energy (kcal/mol)
Glucose	126	126	126	0.742	-19.968, 17.301, -10.987	-3.34

KU80 mouse:

Ligand	X dimension	Y dimension	Z dimension	Spacing	X, Y, Z centre	Binding energy (kcal/mol)
Glucose	126	126	126	0.864	-22.970, -11.432, -14.849	-2.66

KU70 human:

Ligand	X dimension	Y dimension	Z dimension	Spacing	X, Y, Z centre	Binding energy (kcal/mol)
Glucose	126	126	126	0.831	-12.475, -13.679, -23.267	-2.84

KU80 human:

Ligand	X dimension	Y dimension	Z dimension	Spacing	X, Y, Z centre	Binding energy (kcal/mol)
Glucose	126	126	126	0.892	-11.863, 6.259, -27.806	-3.16

Table S4n: POLA1 human and POLA1 mouse:

POLA1 human:

Ligand	X dimension	Y dimension	Z dimension	Spacing	X, Y, Z centre	Binding energy (kcal/mol)
Glucose	126	126	126	0.839	11.952, 10.954, -2.446	-3.58
Psicose	126	126	126	0.858	6.496, 13.357, -6.846	-2.49
Talose	126	126	126	0.842	7.475, 11.577, -7.654	-2.52
Sorbose	126	126	126	0.908	9.764, 9.162, -3.689	2.53
Tagatose	126	126	126	0.847	8.368, 14.330, -5.655	-2.91
Idose	126	126	126	0.936	13.186, 7.346, 1.021	-2.13
Gulose	126	126	126	0.908	8.899, 7.246, -4.268	-2
Allose	126	126	126	0.811	8.038, 0.981, -3.892	-2.62
Altrose	126	126	126	0.797	8.840, 12.468, -6.130	-3.19
Mannose	126	126	126	0.875	9.848, -1.034, -2.080	-3.42
Galactose	126	126	126	0.847	9.241, 6.526, -4.821	-2.23

F16BP	126	126	126	0.908	7.462, 12.116, -4.660	0.68
F6P	126	126	126	0.808	7.252, 11.122, -11.035	-1.26
G6P	126	126	126	0.767	7.903, 1.753, -3.538	-1.41
Fructose	126	126	126	0.836	8.878, 7.303, -5.462	-2.55

POLA1 mouse:

Ligand	X dimension	Y dimension	Z dimension	Spacing	X, Y, Z centre	Binding energy (kcal/mol)
Glucose	126	126	126	0.919	-16.955, 3.070, -6.956	-2.65

Table S4o: ACAA1A mouse and ACAA1A human:

ACAA1A mouse:

Ligand	X dimension	Y dimension	Z dimension	Spacing	X, Y, Z centre	Binding energy (kcal/mol)
Glucose	126	126	126	0.653	-2.398, 0.866, 1.146	-2.82
G6P	126	126	126	0.561	-10.655, -2.473, -3.320	-2.5
F6P	126	126	126	0.531	3.378, 2.037, 1.434	-3.14
F16BP	126	126	126	0.475	-4.432, -2.500, -4.660	-2.67
Mannose (C2)	126	126	126	0.608	-14.287, 1.216, -0.967	-3.91
Galactose (C4)	126	126	126	0.481	-3.786, -0.172, -4.821	-2.93
Altrose	126	126	126	0.469	-0.924, 6.018, 1.119	-3.32
Allose	126	126	126	0.636	-13.876, -3.721, 2.229	-3.48
Gulose	126	126	126	0.606	-10.939, 1.090, -0.499	-3.06
Idose	126	126	126	0.619	-15.024, 5.538, -4.867	-3.88
Talose	126	126	126	0.561	-10.655, -2.473, -3.320	-2.5

Fructose	126	126	126	0.603	-12.376, 0.756, 1.146	-3.43
Psicose	126	126	126	0.686	-14.466, -1.225, -4.800	-3.62
Tagatose	126	126	126	0.664	-14.350, -5.671, -9.467	-3.6
Sorbose	126	126	126	0.619	-14.792, 8.132, -6.581	-2.63

ACAA1A human:

Ligand	X dimension	Y dimension	Z dimension	Spacing	X, Y, Z centre	Binding energy (kcal/mol)
Glucose	126	126	126	0.543	-9.696, 8.947, -14.639	-4.05

Table S5: Binding scores (kcal/mol) of 10 docked conformations of the homologous proteins using Glucose as the ligand.

KIF11 human	-4.15	-3.39	-4.07	-3.59	-3.09	-3.61	-3.2	-3.16	-2.78	-2.29
tKIF11 human	-4.31	-4.21	-3.24	-3.01	-2.99	-2.69	-2.52	-2.65	-2.59	-2.23
CACNB4 human	-4.39	-4.25	-4.3	-3.45	-3.39	-3.25	-3.17	-2.86	-2.61	-2.02
tCACNB4 human	-4.52	-2.86	-4.47	-3.78	-3.15	-3.65	-3.15	-3.02	-2.93	-2.33
ATP6V0A4 human	-4.22	-3.43	-4.07	-3.85	-2.98	-3.58	-2.51	-3.51	-3.14	-3.28
KU70 human	-2.84	-2.57	-2.5	-2.3	-2.09	-1.89	-1.88	-1.75	-1.53	-1.48
KU80 human	-3.16	-2.28	-1.98	-1.95	-1.82	-1.59	-1.26	-1.2	-1.18	-1.11
KU70 mouse	-3.34	-2.69	-2.54	-2.53	-2.49	-2.32	-2.18	-1.96	-1.87	-1.76
KU80 mouse	-2.66	-2.46	-2.44	-2.31	-2.15	-2.06	-1.77	-1.69	-1.57	-1.53
RPA1 mouse	-3.13	-2.7	-3.03	-2.39	-2.32	-2.3	-2.1	-2.1	-2.02	-1.79
POLA1 human	-2.65	-2.18	-2.45	-2.14	-2.02	-1.81	-1.63	-1.13	-1.03	-0.77
ACAA1A human	-4.05	-3.37	-3.34	-3.34	-3.23	-2.3	-3.02	-2.24	-2.2	-1.69
POLR1A mouse	-2.28	-2.18	-1.96	-1.92	-1.6	-1.51	-1.34	-1.02	-0.9	-0.9

Table S6a: Respective conformations, number of interactions and glucose binding scores (kcal/mol) obtained for the test molecules (KIF11, CACNB4, ATP6V0A4) using AutoDock Tools (ADT).

KIF11 mouse			**CACNB4 mouse**			**ATP6V0A4 mouse**		
Conformation	No. of interactions	Binding energy (kcal/mol)	Conformation	No. of interactions	Binding energy (kcal/mol)	Conformation	No. of interactions	Binding energy (kcal/mol)
1	10	-2.91	1	7	-3.37	1	9	-4.09
2	7	-2.91	2	7	-2.56	2	8	-3.53
3	14	-3.81	3	5	-2.72	3	11	-2.69
4	5	-2.18	4	7	-3.11	4	7	-2.69
5	6	-3.16	5	11	-3.87	5	10	-3.46
6	12	-3.8	6	12	-4.19	6	11	-2.98
7	7	-3.47	7	9	-3.79	7	12	-3.92
8	7	-2.08	8	6	-2.78	8	8	-3.71
9	7	-3.3	9	9	-3.17	9	8	-2.94
10	12	-4.62	10	7	-3.25	10	4	-2.39

Table S6b: Respective conformations, number of interactions and glucose binding scores (kcal/mol) obtained for the test molecules (truncated KIF11 and truncated CACNB4) using AutoDock Tools (ADT).

Truncated KIF11 mouse			**Truncated CACNB4 mouse**		
Conformation	No. of interactions	Binding energy (kcal/mol)	Conformation	No. of interactions	Binding energy (kcal/mol)

1	13	-3.51	1	11	-3.43
2	10	-3.17	2	12	-2.48
3	7	-3.15	3	11	-4.46
4	13	-3.06	4	14	-3.66
5	6	-2.94	5	10	-2.54
6	6	-3	6	11	-4.14
7	4	-2.49	7	10	-3
8	10	-2.98	8	12	-2.91
9	11	-4.56	9	5	-2.71
10	11	-3.53	10	10	-3.92

Table S7: Respective conformations, number of interactions and glucose binding scores (kcal/mol) obtained for the positive controls (human and mouse GCK; human and mouse GLUT2, respectively) using AutoDock Tools (ADT).

GCK human			**GCK mouse**		
Conformation	No. of interactions	Binding energy (kcal/mol)	Conformation	No. of interactions	Binding energy (kcal/mol)
1	16	-7.16	1	11	-2.99
2	5	-3.51	2	16	-4.99
3	12	-3.4	3	9	-3.33
4	10	-3.16	4	16	-5.7
5	7	-2.9	5	7	-3.14
6	9	-3.38	6	7	-2.94

7	9	-3.28	7	10	-2.73
8	13	-3.37	8	7	-3.14
9	11	-2.93	9	8	-3.02
10	15	-5.29	10	5	-2.51
GLUT2 mouse			**GLUT2 human**		
Conformation	No. of interactions	Binding energy (kcal/mol)	Conformation	No. of interactions	Binding energy (kcal/mol)
1	11	-4.35	1	13	-3.71
2	11	-3.22	2	10	-3.5
3	16	-5.04	3	9	-4.64
4	11	-4.18	4	9	-4.64
5	16	-5.01	5	8	-2.64
6	11	-3.32	6	13	-4.22
7	8	-3.22	7	9	-3.83
8	7	-3.04	8	15	-3.41
9	16	-5.35	9	11	-3.53
10	16	-5.23	10	10	-3.74

Table S8a: Respective conformations, number of interactions and glucose binding scores (kcal/mol) obtained for the negative controls (RPA1, KU70-80, POLR1A, ACAA1A) using ADT, as tabulated below:

RPA1 human			**KU70-80 human**		
Conformation	No. of interactions	Binding energy	Conformation	No. of interactions	Binding energy
1	10	-3.28	1	10	-2.46
2	8	-2.67	2	8	-2.62
3	7	-2.29	3	4	-1.81
4	11	-3.81	4	7	-2.55
5	6	-1.84	5	10	-2.42
6	10	-2.28	6	7	-1.21
7	6	-2.57	7	12	-1.98
8	9	-2.26	8	14	-3.16
9	10	-3.19	9	14	-3.75
10	10	-3.42	10	9	-2.65
POLR1A human			**ACAA1A mouse**		
Conformation	No. of interactions	Binding energy	Conformation	No. of interactions	Binding energy
1	8	-2.05	1	7	-2.82
2	6	-1.05	2	6	-1.95
3	8	-1.9	3	8	-2.82
4	11	-2.52	4	7	-2.55
5	5	-2.31	5	7	-2.43

6	7	-1.6	6	9	-1.62
7	8	-2.66	7	7	-2.75
8	4	-1.04	8	8	-2.16
9	8	-2.27	9	8	-2.49
10	5	-1.35	10	6	-2.63

Table S8b: Respective conformations, number of interactions and glucose binding scores (kcal/mol) obtained for the negative control POLA1 using ADT, as tabulated below:

POLA1 human		
Conformation	No. of interactions	Binding energy
1	4	-1.1
2	9	-2.2
3	8	-1.51
4	13	-3.58
5	8	-1.34
6	7	-2.11
7	10	-2.24
8	9	-3.47
9	5	-1.51
10	10	-2.32

Table S9: Calculation of Pearson's correlation co-efficient - The binding energies (kcal/mol) and the number of interactions for the respective conformations within a single protein was noted. This was done for every other protein molecule used. Pearson's correlation coefficient (r) was calculated between the obtained binding energies (kcal/mol) and the number of interactions for the respective conformations within a single protein, and for every other protein molecule used.

Protein	Correlation co-efficient
KIF11 mouse	-0.719295178
CACNB4 mouse	-0.876733384
ATP6V0A4 mouse	-0.451581861
Truncated KIF11 mouse	-0.56571539
Truncated CACNB4 mouse	-0.270182629
GCK mouse	-0.888238606
GCK human	-0.707709324
GLUT2 mouse	-0.921812214
GLUT2 human	0.042588125
RPA1 human	-0.730916906
KU70-80 human	-0.684584588
POLA1 human	-0.776573019
POLR1A human	-0.684089168
ACAA1A mouse	0.334563411

Table S10: Visualisation of the binding propensity of D-glucose: The highest binding energy scores corresponding to the respective conformation of the protein molecule along with the orientation or the binding propensity of the docked ligand are shown.

Protein	Structure	Conformation with the highest binding energy	Binding propensity of ligand	Binding energy (kcal/mol)
KIF11 mouse	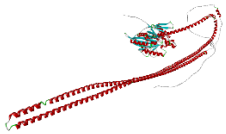	10	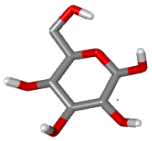	-4.62
Truncated KIF11 mouse (90-400)	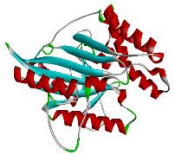	9	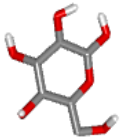	-4.56
CACNB4 mouse	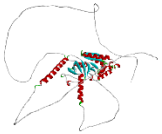	6	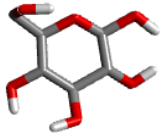	-4.19
Truncated CACNB4 mouse (60-450)		3	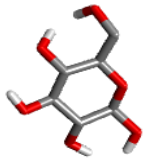	-4.46
ATP6V0A4 mouse		1	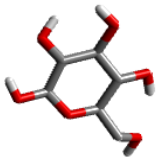	-4.09

GCK mouse	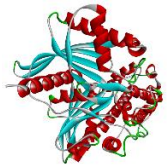	4	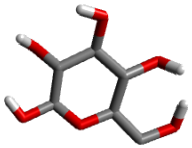	-5.70
GCK human		1	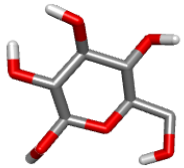	-7.16
GLUT2 mouse		9	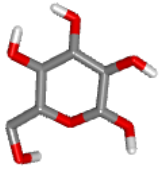	-5.35
GLUT2 human		3,4	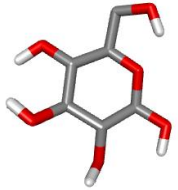	-4.64
RPA1 human		4	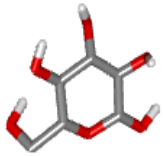	-3.81
KU70-80 human	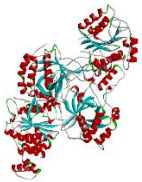	9	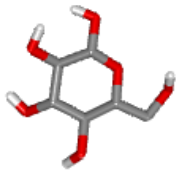	-3.75

POLA1 human	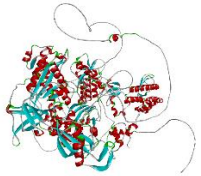	4	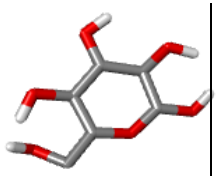	-3.58
ACAA1A mouse	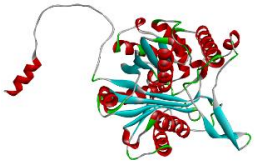	1,3	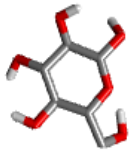	-2.82
POLR1A human	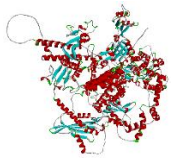	7	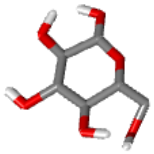	-2.66

Table S11: All the ligands used for binding studies have been tabulated below with their respective PubChem CID's:

Ligand	PubChem CID (https://pubchem.ncbi.nlm.nih.gov/)
D-Glucose	5793
D-G6P	5958
D-F6P	440641
D-F16BP	172313
D-Mannose	18950
D-Galactose	6036
D-Altrose	441032
D-Allose	439507
D-Gulose	441033
D-Idose	441034
D-Talose	441035
D-Fructose	2723872
D-Psicose	441036
D-Tagatose	439312
L-Sorbose	439192

Table S12: The highest binding scores (kcal/mol) obtained with the test proteins using glucose as the ligand were statistically compared with the highest binding scores (kcal/mol) obtained with the test proteins for every other ligand apart from glucose, using two-tailed Student's t-test assuming equal variances. The p-values thus obtained are tabulated below:

	Ligand	Equal var P(T<=t) two-tail
Comparison of glucose binding scores (kcal/mol) of test proteins VS	G6P	0.00595901
	F6P	0.009226493
	F16BP	6.57195E-06
	Mannose	0.021289143
	Galactose	0.008635834
	Altrose	0.014700714
	Allose	0.030293155
	Gulose	0.000788729
	Idose	0.005714733
	Talose	0.001341974
	Fructose	0.001461657
	Psicose	0.000924343
	Tagatose	0.000891943
	Sorbose	0.000727152

Table S13a: Homologous proteins belonging to the same protein sets (test proteins, positive controls, and negative controls, respectively) were chosen that were previously not used for glucose binding studies, and then binding studies were done specifically using glucose as the ligand for comparison. The glucose binding scores as obtained are tabulated below:

Protein	Glucose binding score (kcal/mol)
Intact KIF11 human	-4.15
tKIF11 human (90-400)	-4.31
Intact CACNB4 human	-4.39
tCACNB4 human (60-450)	-4.52
ATP6V0A4 human	-4.22
KU70 mouse	-3.34
KU70 human	-2.84
KU80 mouse	-2.66
KU80 human	-3.16
POLA1 mouse	-2.65
ACAA1A human	-4.05
RPA1 mouse	-3.13
POLR1A mouse	-2.28

Table S13b: Statistical analyses of glucose binding scores (kcal/mol) between homologous proteins of the same sets. The binding scores of the test proteins of a particular species were statistically compared with the binding scores of positive controls, negative controls, and in between positive and negative controls respectively, of the same species. This was repeated for the other species too. Then, similar proteins from two different species but belonging to the same set were statistically compared too. The statistical analyses were done through two-tailed Student's t-test assuming equal variances. The p-values thus obtained are tabulated below:

Protein type	Comparison of protein sets	Equal var P(T<=t) two-tail
Human	Test protein – Positive control	0.066212
	Test protein – Negative control	0.00397
	Positive control – Negative control	0.007268
Mouse	Test protein – Positive control	0.002171
	Test protein – Negative control	2.06E-05
	Positive control – Negative control	9.02E-05

Human vs Mouse	Test human – Test mouse	0.604868
	Positive human – Positive mouse	0.795939
	Negative human – Negative mouse	0.042298
	Positive human – Negative mouse	0.003338
	Positive mouse – Negative human	0.001098
	Test human – Positive mouse	0.000377
	Test mouse - Positive human	0.079092
	Test human – Negative mouse	0.000015
	Test mouse – Negative human	0.003227

Table S14: Different insulin secreting model systems obtained from different species used to study GSIS:

S. No.	Cells	Doubling time	Passage No.	Source and Species	Methods	Stimulus behind insulin secretion	Extent of Insulin secretion or total Insulin content	Type of Insulin Assay	GSIS response	Role of glucose behind GSIS (extracellular or intracellular)	References
1.	HIT	~ 34 h	37	Hamster insulinoma	SV40 T-antigen transfected hamster pancreatic islet cells	Stimulation with media containing 7.5 mM glucose for 1 h at 37ºC	2.4 mU/10^6 cells/h	RIA	Low GSIS response as compared to hamster islet monolayer cultures. A 2-fold increase in insulin secretion was observed at 7.5 mM glucose as compared with 1.25 mM glucose stimulus	Extracellular	[44]
2.	Hamster islets	-	-	Syrian hamster	As per islet isolation protocol	Stimulation with media containing 7.5 mM glucose for 1 h at 37ºC	110.4 mU/10^6 cells/h	RIA	A 6.8-fold increase in insulin secretion was observed at 7.5 mM glucose stimulus as compared with 1.25 mM glucose stimulus	Extracellular	[44]
3.	Rat islets	-	-	Rat	As per islet isolation protocol	Stimulation with Krebs-Henseleit bicarbonate media containing 20 mM glucose for 2 hr at 37 ºC	281 pg/islet/min	RIA	A 2.1-fold increase in GSIS was observed at 20 mM glucose as compared to 5.5 mM glucose stimulus	Extracellular	[63]
4.	Mouse islets	-	-	Mouse	As per islet isolation protocol	Stimulation with Krebs-Henseleit bicarbonate media containing 20 mM glucose for 2 hr at 37 ºC	203 pg/islet/min	RIA	A 4.8-fold increase in GSIS was observed at 20 mM glucose as compared to 5.5 mM glucose stimulus	Extracellular	[63]
5.	Mouse islets	-	-	FVB and C57BL/6J mice	As per islet isolation protocol	Stimulation with media containing 16.7 mM glucose for 1 h at 37ºC	Insulin secreted was calculated in terms of (ng/100 IEQ's/ min); (ng/islet/24h), and AUC as (ng/100 IEQ's)	RIA	Mouse islets secreted more insulin at 16.7 mM glucose alone and with 3-isobutyl-1-methylxanthine. A 30-fold increase in GSIS was observed at 16.7 mM glucose as compared with basal stimulus of 5.6 mM glucose	Extracellular	[64]

6.	Human islets	-	-	Male and female human cadavers	As per islet isolation protocol	Stimulation with media containing 16.7 mM glucose for 1 h at 37ºC	Insulin secreted was calculated in terms of (ng/100 IEQ's/ min); (ng/islet/24h), and AUC as (ng/100 IEQ's)	RIA	Human islets secreted more insulin than mouse islets at 5.6 mM glucose but secreted lesser insulin at 16.7 mM glucose alone and with 3-isobutyl-1-methylxanthine. A 3-fold increase in GSIS was observed at 16.7 mM glucose and a 5-fold increase in GSIS with 16.7 mM glucose and IBMX, as compared with basal stimulus of 5.6 mM glucose	Extracellular	[64]
7.	INS-1	~ 100 h	45	Rat insulinoma	Induced by X-ray radiation	Stimulation with KRBH containing 20 mM glucose for 30 min at 37 ºC	8 µg/10^6 cells	RIA	The insulin content was 20% of the native β-cell content, only 2 to 4-fold increase in insulin secretion was seen as opposed to 15-fold increase with freshly isolated primary islets	Extracellular	[45]
8.	INS1 832/13 cells	81.81 h	66	Rat insulinoma	Parental INS-1 cells were transfected with the plasmid pCMV8/INS/IRES/Neo containing human insulin cDNA	Stimulation with HBSS containing 15 mM glucose for 2 hr at 37 ºC	800 ng/mg protein/hr	RIA	The insulin content was 1.5 µg/10^6 cells, a 10-fold increase in insulin secretion at 15 mM glucose was observed as compared with 3 mM glucose stimulus	Extracellular	[46]
9.	INS-1E	166 h	27-142	Isolation of clonal INS-1E cells from parental rat INS-1 cells	Cloning of well differentiated INS-1 cells	Stimulation with KRBH containing 20 mM glucose for 30 min at 37 ºC	3.46 µg insulin/10^6 cells at passage 64	RIA	The average insulin content was 2.3 µg/10^6 cells, which is 10% of the content of native rat β-cells. Also, a 15 mM-20 mM glucose stimulation resulted in a 6.2-fold change in secreted insulin	Extracellular	[47]
10.	MIN6	~ 48 h	15	Mouse insulinoma	Human insulin promoter connected to the SV40 was microinjected in	Stimulation with 25 mM glucose for 12 h at 37 ºC	275 mU/10^6 cells/24h or 11.45 mU/10^6 cells/h	RIA	GSIS comparable to that of mouse islet cells, a 9.8-fold increase in insulin secretion was observed as compared to the secretion at 5 mM	Extracellular	[26]

					the pronuclei of fertilized eggs of C57BL/6 mice				glucose stimulus		
11.	βTC-1	~ 58 h	50	Mouse insulinoma	SV40 T-antigen transgenic mouse	Stimulation with KRBH containing 5.6 mM glucose for 12 h at 37 ºC	43.7 mU/10^6 cells/24h or 1.8 mU/10^6 cells/h	RIA	Not responsive to glucose stimulation beyond 5.6 mM. The insulin content was 4 mU/10^6 cells	Extracellular	[52]
12.	βTC-6	-	36	Mouse insulinoma	SV40 T-antigen transgenic mouse	Stimulation with media containing 5.6 mM glucose for 2 h at 37 ºC	50 pmol/mg protein or 5280 pmole/L	RIA	Secrete 11 times and 4 times more insulin at basal and 5.6 mM glucose stimulus respectively, as compared to HIT-T15 cells	Extracellular	[53]
13.	NIT-1	~ 49 h	16	Mouse insulinoma	Transgenic NOD/Lt mouse	Stimulation with media containing 16.5 mM glucose for 70 minutes at 37 ºC	Insulin content: 638 ng/10^6 cells Insulin secreted: 103 ng/10^5 cells/h or 2.94 mU/10^5 cells/h	RIA	At passage 11 and 16, NIT-1 cells showed glucose responsiveness to both 11- and 16.5-mM glucose stimulus respectively, but it was diminished at passage 19	Extracellular	[54]
14.	BRIN-BD11	~ 20 h	12-25	Rat pancreatic islet cells and insulinoma	Electrofusion	Stimulation with media containing 11.1- and 33.3-mM glucose for 24 h at 37 ºC	320 ng/10^6 cells/24h or 0.38 mU/10^6 cells/h	RIA	Exhibits GSIS in the physiological range. An increase of 1.8- and 2-fold insulin secretion was observed at 11.1- and 33.3-mM glucose stimulus respectively, as compared to 1.4 mM glucose stimulus	Extracellular	[48]
15.	RINr	~ 52 h	20	Rat insulinoma	Induced by radiation	Stimulation with culture media containing 16.5 mM glucose at 37 ºC	Maximum at 100 µU/10^6 cells/24h or $0.41*10^{-2}$ mU/hr	RIA	Not determined	Extracellular	[49]
16.	RINm	~ 72 h	6	Rat insulinoma	Induced by radiation	Stimulation with media containing 16.5 mM glucose at 37 ºC	200 µU/10^6 cells/24h or $0.83*10^{-2}$ mU/hr	RIA	Not determined	Extracellular	[49]
17.	RINm5F	~ 48 h	--	Rat insulinoma	Induced by radiation	Stimulation with KRBH containing 16.7 mM glucose for 0.5-1 h at 37 ºC	Insulin content: 191 ng/10^6 cells, Insulin secreted: 10.6 ng/10^6 cells/h or 0.29 mU/10^6 cells/h	RIA	No change in insulin secretion throughout 2.8 – 33.4 mM glucose concentrations	Extracellular	[50]

18.	EndoC-βH1	~ 120 h	25-40	Human foetal pancreas	Transduction of foetal pancreas with SV40LT under the control of insulin promoter and grafted into SCID mice with vector expressing hTERT	Stimulation with KRBH containing 20 mM glucose for 1 h at 37 ºC	Insulin content: 0.46 µg/10^6 cells Insulin secretion: 5.96 ng/10^6 cells/h at 0.5 mM glucose and 19.29 ng/10^6 cells/h at 20 mM glucose	ELISA	Response within physiological range, showing a 3.23-fold change increase in insulin secretion	Extracellular	[57,58]
19.	CRI-G1	--	--	Rat insulinoma	Radiation induced	Stimulation with media containing 16.7 mM glucose for 1 h at 37 ºC	Insulin content: 1-90 pmol/10^6 cells Insulin release: 6-250 pmol/10^6 cells/24h	RIA	No change in insulin secretion throughout 2.8 mM to 16.7 mM glucose concentrations	Extracellular	[51]
20.	βlox5	--	--	Human foetal pancreas	SV40 T-antigen, H-ras^{val12}, hTERT oncogene	Stimulation with media containing 22 mM glucose for 1 h at 37 ºC	Insulin content: 6-21 pmol/µg DNA/hr	RIA and ELISA	Responsive within a range of 0-22 mM glucose concentration, but with low insulin content	Extracellular	[59]
21.	IgSV195	18 h	--	Mouse insulinoma	SV40 T-antigen transgenic mouse	Stimulation with media containing 25 mM glucose along with dialyzed FBS for 1 h at 37 ºC	993 pM/4*10^5 cells	RIA	Not responsive within a range of 0-25 mM glucose concentration unless treated with dialyzed FBS or a combination of 3-isobutyl-1-methylxanthine and glutamine	Extracellular	[55]
22.	βHC9	--	--	Mouse hyperplastic islets	SV40 T-antigen transgenic mouse	Stimulation with Hanks-BSA solution containing 15 mM glucose for 2 h at 37 ºC	20-21 mU/10^6 cells	RIA	Responds to glucose stimulation within a range of 0-25 mM, unlike the other clones. A 40-fold increase in insulin secretion was observed at 25 mM glucose stimulus as compared to 0.1 mM glucose stimulus	Extracellular	[56]
23.	CM	--	--	Human Insulinoma	Ascitic fluid of liver metastasis of malignant insulinoma	Stimulation with KRBH containing 22 mM of glucose for 4 h at 37 ºC	Negligible	RIA	Not responsive within a range of 0-22 mM glucose concentration	Extracellular	[60]

24.	TRM-1	36 h	--	Human foetal pancreas	SV40 T-antigen, H-ras^{val12}	Stimulation with 20 mM of glucose at 37 ºC	Low levels of insulin	RIA	Not responsive to glucose stimulation	Extracellular	[61]
25.	NAKT-15	--	--	Human pancreatic β-cells	SV40 T-antigen and hTERT cDNA transgenic mouse with Cre-LoxP based reversible immortalization	Stimulation with media containing 25 mM of glucose for 1 h at 37 ºC	Insulin content: 4.83 ng/g protein Insulin secretion: 37.8 ng/mg protein at 5.6 mM glucose to 298.6 ng/mg protein at 25 mM glucose	ELISA and RIA	Dose dependent response to glucose was seen, a 7.9-fold increase in insulin secretion at 25 mM glucose stimulus was observed as compared to 5.6 mM glucose stimulus	Extracellular	[62]
Other cells engineered to produce Insulin											
26.	Intestinal epithelial cells	--	--	C57BL/6 foetal mice	Incubation of intestinal epithelial cells with GLP-1 (1–37) at 10 nmol/litre for 8 days	Stimulation with media containing 25 mM glucose for 2 h at 37 ºC for 8 days	Insulin content: 88.9 ng/well or 2.54 mU/10^6 cells	ELISA	GLP-1 (1-37) along with 25 mM glucose resulted in enhanced insulin secretion as compared to either of them	Extracellular	[42]
27.	Caco-2 epithelial cells	62 h	--	Human epithelial colorectal adenocarcinoma	*Escherichia coli* Nissle strain expressing either PDX-1 or GLP-1	16 h incubation with cell-free media from overnight cultures of engineered Nissle strains followed by 0.4% or 22.2-mM glucose stimulation for 2 h	Insulin secretion: a) GLP-1 with glucose: 1 ng/mL b) PDX-1 with glucose: 0.5 ng/mL c) GLP-1 and PDX-1 with glucose: 0.5 ng/ml d) Synthesised GLP-1 (1-37) with glucose: 0.8 ng/mL	ELISA	22.2 mM glucose along with GLP-1 resulted in a 2-fold enhanced insulin secretion as compared to 22.2 mM. glucose with PDX-1. Combining both along with 22.2 mM glucose didn't alter the level of secreted insulin	Extracellular	[43]

Docking pipeline:

Glucose binding analyses using AutoDock Tools 4.2.6 (ADT) and subsequent visualization of the docked conformations through Discovery Studio 2021 (DS): The exact methodology and pipeline used in ADT and DS has been mentioned below.

a. Initializing the protein molecule:

1. File ➡ Read Molecule ➡ Open the protein structure in .pdb format.
2. Delete water molecules: Edit ➡ Delete water.
3. Add hydrogens: Edit ➡ Hydrogens ➡ Add ➡ Polar only.
4. Merge non-polar hydrogens: Edit ➡ Hydrogens ➡ Merge Non-polar.
5. Add charges: Edit ➡ Charges ➡ Add Kollman charges.
6. Assign atoms: Edit ➡ Atoms ➡ Assign AD4 type.

b. Initializing the ligand:

1. The 3D conformer of the ligand (D-glucose) was downloaded from the PubChem database (https://pubchem.ncbi.nlm.nih.gov/), CID – 5793, in '.sdf' file format.
2. Using Open Babel GUI (, the file format of the ligand was converted from '.sdf' (input format to '.pdb' (output format), for further processing in AutoDock Tools 4.2.6.
3. Ligand ➡ Input ➡ Open (ligand filename in '.pdb' format)
4. A display box will appear showing ligand setup, the addition of Gasteiger charges, number of non-polar hydrogens merged, number of rotatable bonds detected, and number of torsional degrees of freedom detected (TORSDOF).
5. Detect the central atom in ligand: Ligand ➡ Torsion tree ➡ Detect Root.
6. Detect the number of active bonds: Ligand ➡ Torsion tree ➡ Choose Torsion
   ➡ Number of rotatable bonds ➡ Done.
7. Save the ligand file in .pdbqt format: Ligand ➡ Output ➡ Save as .pdbqt file.
8. Since the ligand (D-glucose) for all the binding analyses was same, this 'glucose.pdbqt' file was directly used as the input file in Step 3 for subsequent glucose docking analyses, instead of manual initialization of 'ligand.pdb' file as stated above.

c. Preparation of the protein macromolecule and ligand:

1. Select the macromolecule: Grid ➡ Macromolecule ➡ Choose ➡ Select molecule ➡ A display box will appear showing 'initializing protein.pdb:

contains no non-bonded atoms' ➡ Ok ➡ Type and save the filename in .pdbqt format. The colour of the macromolecule will change.

2. Select the ligand: Grid ➡ Set map types ➡ Choose Ligand ➡ Select molecule ➡ Select ligand.

d. Setting up grid box parameters:

1. Grid ➡ Grid box. The grid parameters chosen for all the protein molecules have been tabulated in Supplementary tables S6a to S6o.
2. Save the Grid box parameters: File ➡ Close saving current.

e. Preparing the AutoGrid parameter file:

1. Grid ➡ Output ➡ Save GPF ➡ Type the filename and save as '.gpf' format.

f. Running the AutoGrid:

1. Run ➡ Run AutoGrid ➡ Program pathname file: C:/Docking/autogrid4.exe
2. Parameter filename ➡ Select and open the 'protein.gpf' filename (C:/Docking/protein.gpf)
3. Log filename ➡ A new grid log file (C:/Docking/protein.glg) will be created. ➡ Launch.

g. Preparing the AutoDock parameter file:

1. Select the gridmap file: Docking ➡ Macromolecule ➡ Set rigid filename ➡ Select the 'protein.pdbqt' macromolecule file.
2. Select the ligand: Docking ➡ Ligand ➡ Choose ➡ Select molecule ➡ Select ligand.
3. Search Parameters: Docking ➡ Search parameters ➡ Genetic Algorithm ➡ Accept.
4. Docking parameters: Docking ➡ Docking parameters ➡ Accept.
5. Output file: Docking ➡ Output ➡ Lamarckian GA ➡ Save the docking parameter output file as 'protein.dpf' format.

h. Running the AutoDock:

1. Run ➡ Run AutoDock ➡ Program pathname file: C:/Docking/autodock4.exe
2. Parameter filename ➡ Select and open the 'protein.dpf' filename (C:/Docking/protein.dpf)
3. Log filename ➡ A new docking log file (C:/Docking/protein.dlg) will be created. ➡ Launch.

i. Docking result analysis from docking parameter log file:

1. Using AutoDockTools:
    a. Analyze ➡ Dockings ➡ Open ➡ Select the ‘protein.dlg’ file (docking parameter log file).
    b. A display box will appear showing the number of docked conformations from ‘protein.dlg’ file .
    c. Analyze ➡ Macromolecule ➡ Open. The protein structure gets displayed.
    d. Analyze ➡ Conformations ➡ Play ➡ Select the ‘&’ menu.
    e. Click on ‘Show info’ and ‘Build H-bonds’ ➡ Among others, note the binding energy for each conformation.
    f. Click on ‘Write complex’ to save the respective conformation of the protein-ligand complex as a ‘.pdbqt’ file.
    g. Repeat steps E and F for 10 ligand conformations computed for a single protein.
2. Using Discovery Studio Visualiser 2021:
    a. Select the respective conformation of the protein-ligand complex: Discovery Studio ➡ File ➡ Open ➡ ‘All files’ ➡ Select the protein-ligand complex in ‘.pdbqt’ file format that was previously saved in AutoDock.
    b. Change the display style: Scripts ➡ Visualisation ➡ Publication quality. Display style ➡ 2nd option.
    c. Save the protein-ligand complex with the chosen display settings as a ‘.dsv’ file (Discovery studio file).
    d. Save the protein-ligand complex with the chosen display settings as a ‘.png’ file (Image file).
    e. Viewing the number of interactions: Show receptor-ligand interactions on a 2D diagram ➡ Show 2D diagram.
    f. Save the 2D diagram as a ‘.png’ file (Image file).
    g. Deselect the ‘Protein groups’ and save the propensity of the docked ligand as a ‘.png’ file (Image file).
    h. Steps A to G were performed for each conformation of the protein-ligand complex for a particular protein, and subsequently for every other protein molecule used.